MECHANISM OF COLLOIDAL SPHERE SELF-ASSEMBLY

TIAN HUI ZHANG

(B.Sci, Central China Normal University, Wuhan, China)
(M.Sci, Institute of Physics, Chinese Academy of Sciences, Beijing, China)

A THESIS SUBMITTED

FOR THE DEGREE OF DOCTOR OF PHILOSOPHY

DEPARTMENT OF PHYSICS

NATIONAL UNIVERSITY OF SINGAPORE

2008

Acknowledgements

First and foremost, I would like to express my deepest and sincere gratitude to my supervisors: Professor Xiang Yang Liu and Professor Bao Wen Li. This work would not have been possible without their guidance and assistance. Professor Liu's wide knowledge and his logical way of thinking have been of great value to me. His encouragement and personal guidance have offered me the most valuable support throughout my Ph.D student life. Without this sort of support, it would be hard to imagine that I could find enough courage to take these challenges facing me in my study and complete this work. I could not have expected a better advisor and mentor for my Ph. D work.

I would also like to thank Dr. Christina Strom for helping me throughout the period of my research by providing advice, support and editing the papers and this thesis. I would also like to express my sincere gratitude to Dr. Claire Lesieur and Yan Jie for their advice and practical instruction in biology.

In the course of my research, I have had the opportunity to interact with many people, and learn a lot from each of them. Here, I would like to thank my lab mates and friends, Huaidong, Keqing, Du Ning, Yanwei, Yanhua, Junying, Jingliang, Rongyao, Liu Yu, Junfeng, Zhou Kun. Special thanks are due to Mr. Teo, Eric and Low Yee Teck for their support and help throughout my research work.

I am indebted to my parents and my sister for their love and support throughout

my life. My parents have always done their best to support and encourage me since my schooldays as a child. It is their love and encouragement that took me through so many difficulties and challenges in my life. I am deeply grateful to my sister. She has taken the duty to take care of my parents in these years so that I can focus on my study.

I would like to give my special thanks to my beloved wife Lingling Song for her love and patience during the PhD period. Her patient love and support enabled me to complete this work.

At last, I will give my acknowledgement to National University of Singapore for offering the scholarship to support my study.

Table of Contents

Summary

Crystallization is a widespread phenomenon in the inanimate world and living organisms. This process has been employed as a major strategy in developing electronic, optical and magnetic materials. Therefore, the study of crystallization is one of the most important areas of condensed matter physics, materials science and biological science. In the study of crystallization, the pathway for crystal nuclei to approach their final stable crystalline structure is of fundamental importance.

The *in-situ* observation in a colloidal model system suggests that due to surface effects, crystal nuclei emerge with a liquid-like structure at the early stage and develop a crystalline core in subsequent growth, with the liquid component being maintained in the exterior layer of the nuclei. Crystal nuclei become entirely crystalline only when they reach a critical size. In this process, the nuclei structure is size dependent and the average order degree rises gradually with the size of the nuclei. As a consequence of the liquid exterior, the nucleation barrier is reduced compared with the prediction of classical nucleation theory (CNT).

An alternative pathway for crystal nucleation is multi-step crystallization (MSC). In our experiments, it was found that under certain conditions, the first nucleated phase is a metastable amorphous phase. Crystalline nuclei subsequently nucleate from the metastable phase. Sub-crystalline nuclei in the metastable phase nucleate by structure fluctuations, consistently with CNT. However, the critical crystalline nuclei

in the metastable amorphous phase are formed by coalescence of the sub-crystalline nuclei. An amorphous cluster can accommodate only one stable crystalline nucleus. The structure and density decrease continuously from the crystalline core to the amorphous fringe. The continuous decrease in structure and density has kinetic advantages in producing perfect crystals.

To determine the nucleation rate of crystals in the metastable amorphous phase, a mathematical method is developed. The experimentally determined nucleation rates enable us to measure the relative supersaturation for crystallization and the crystal-liquid interface energy in the metastable amorphous phase.

After the nucleation stage, postcritical crystal nuclei grow into bulk crystals through incorporation. It has been found that, due to the attraction between the incoming atoms and the step atoms, the incoming atoms are preferentially absorbed by step protrusions, the so-called steering effect, giving rise to the growth instability and the formation of mounds. However, our observations in the colloidal model system reveal that the steering effect reflects only one side of the story. The attraction can also cause additional interlayer mass transport, resulting in a smoothing effect. The smoothing effect will become significant when the step protrusions are small. Such is the case in the growth of films by low temperature epitaxy. The smoothing effect identified in our experiments may interpret the experimentally observed reentrant two-dimensional growth of thin films at low temperatures.

In our experiments, colloidal crystals are employed as a model for atomic materials to study the properties of defects. In our studies, various vacancies are investigated. It is found that monomer vacancies are immobile and have identical symmetry with the underlying triangular lattice. Both dimer vacancies and trimer vacancies have two different configurations and the configurations with higher symmetry are more stable. Dimer vacancies in our experiments exhibit the highest diffusivity, whereas the global diffusion of vacancies of larger clusters, such as trimer vacancies, is inhibited. Compared with previous studies, it is found that defect dynamics is strongly dependent on the nature of the interaction potential.

List of Figures

Abbreviations and Symbols

CNT Classical nucleation theory

TSC Two step crystallization

MSC Multistep crystallization

AEF Alternating electric field

EHD Electrohydrodynamic

2DC Two dimensional crystal

3DC Three dimensional crystal

3DL Three dimensional liquid

3DDA Three dimensional disordered aggregation

N Number of colloidal particles in a colloidal cluster

N^* Critical size for an amorphous droplet in MSC to create a stable crystal nucleus

N_{crys} Number of crystal-like particles in colloid cluster

N^*_{crys} Critical size for crystal nuclei formed in the amorphous droplet in MSC

A(t) Area of a 2D colloidal cluster

τ The time needed for an amorphous droplet in MSC to reach its critical size N^*

d_0 The average distance between two nearest liquid-like particles in a colloidal cluster

d_c The average distance between two nearest crystal-like particles in a colloidal cluster

c_m The equilibrium concentration for a colloidal cluster in MSC, below which crystal nuclei can not be formed from the amorphous droplets

d_m The average distance between two nearest neighbor particles when the

concentration in the colloidal cluster is c_m

γ Interface tension or surface free energy

Publications

[1] T. H. Zhang, X. Y. Liu, **submitted.**
Size Dependence of the Structure of Precritical Crystal Nuclei

[2] T. H. Zhang, X. Y. Liu, **J. Phys. Chem. B,** 111, 14001(2007).
Multistep Crystal Nucleation: A Kinetic Study Based on Colloidal Crystallization

[3] T. H. Zhang, X. Y. Liu, **J. Am. Chem. Soc.** 129, 13520 (2007).
How Does a Transient Amorphous Precursor Template Crystallization

[4] T. H. Zhang, X. Y. Liu, **J. Phys. Chem. C** 111, 1342 (2007)
Effect of Long-Range Attraction on Growth Model

[5] T. H. Zhang, X. Y. Liu, **Appl. Phys. Lett.** 89, 261914 (2006)
Configurations and Diffusion of Point defects in Two-Dimensional Colloidal Crystals

Chapter 1 Introduction

1.1 Crystallization

1.1.1 Crystallization in Nature and Technology

Crystals are solids with atoms arranged in a regular three-dimensional periodic pattern. Crystallization is the process of forming crystals from solutions, melts or vapor. This process is widespread in nature and of great importance in technology.

In nature, crystallization occurs widely in the inanimate world and living organisms. The most often observed example of crystallization in nature and our everyday life is the crystallization of water, which forms ice such as snow flakes (Figure 1.1) from supercooled water. Another important category of crystallization in nature is the formation of minerals which offers human beings a number of necessary resources including chemicals, metals and semiconductors. In living organisms, crystallization plays a key role in producing crystalline materials which have specific

functions. For instance, magnetite crystals synthesized by magnetic bacteria help bacteria navigate in the earth's magnetic field [1]; calcite and aragonite, the crystalline form of calcium carbonate created by crystallization, are produced to serve as gravity sensors by land and sea animals [2]. Other examples of functional biological materials formed through biomineralization include bone, teeth and shells.

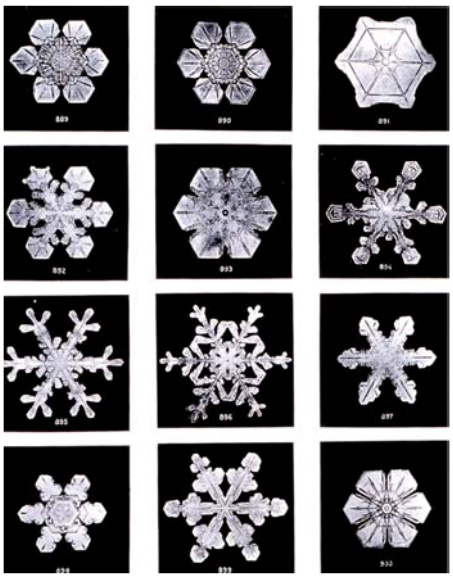

Figure 1.1 Snow flakes

In technology, crystallization plays a central role in many technological applications. For instance, to fabricate advanced optical, electronic and magnetic devices, large-scale bulk crystals, such as single silicon crystals, have to be prepared by crystallization. Moreover, high-quality crystalline films, which are the critical component of transistors and thus are the foundation of computer and information technology, are also universally prepared by crystallization. Furthermore, in

biotechnology, the knowledge of the structure of proteins is the key for drug design [3] and disease treatment [4, 5]. In practice, protein crystals have to be prepared by crystallization for the use of X-ray crystallography which is the most widely employed method [3, 6] of determining the structure of proteins.

1.1.2 Crystallization Control

In nature, the crystals produced by biomineralization are essentially uniform in size and identical in morphology [1-2], which is impossible without control over the crystallization processes, suggesting that organisms have a strong capability in controlling crystallization. In biological sciences, this sort of capability is highly desirable. For instance, large protein crystals of high-quality are critical for the determination of the structure of proteins by X-ray crystallography. In this case, enhancing protein crystallization is of great interest in practice. Unfortunately, it is still a hard task in biotechnology [7, 8]. On the other hand, it has been found that protein crystallization is responsible for diseases such as human genetic cataract [4], Alzheimaer's disease, Parkinson's disease and Huntington's disease [5]. In these cases, inhibiting protein crystallization is desirable. Consequently, controlling crystallization, including promoting protein crystallization as well as to suppressing protein crystallization, depending on the case is critical in practice.

In material science, the typical size of devices has been reduced down to the

nanometer scale; nano crystal structures are playing a key role in developing novel electronic, photonic and magnetic devices. At the nanometer scale, the morphology, shape and size of nano crystals have strong impact on the properties of devices. Consequently, precise control on the process of crystallization is critical in nanotechnology [9-11].

From the above review, we can see that control of crystallization is widely desirable in technology. However, a precise control of crystallization as observed in living organisms is impossible before a complete quantitative understanding of crystallization is achieved. Furthermore, a comprehensive understanding of crystallization may lead to a new class of functional solids based on self-assembly of designed growth units.

In the last century, the combination of theoretical studies and experimental studies has borne several theoretical models dictating crystallization, including classical nucleation theory, Ostwald's rule and two-step crystallization.

1.1.2 Understanding Crystallization

Crystallization is a typical first-order phase transition. The thermal driving force of crystallization is the fact that the atoms in the bulk crystal phase have a lower chemical potential than that in the mother phase; therefore, the mother phase is metastable with respect to the crystalline phase.

Crystallization begins with the so-called nucleation by which crystal embryos or

nuclei are created from thermal fluctuations. Stable crystal nuclei formed by nucleation would serve as substrates for the subsequent crystal growth which proceeds by incorporating adatoms at kink sites.

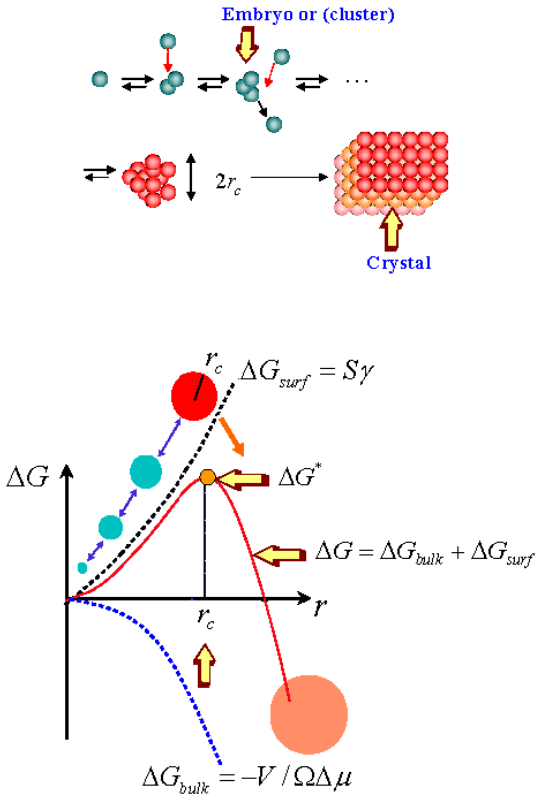

Figure 1.2 Due to the competition between the reduced bulk free energy and the increased surface free energy, there is a nucleation energy barrier and thus a critical size of the crystal nuclei.

1.2 Nucleation

Nucleation is the earliest stage of crystallization. It has been studied for more than a century. The first theoretical work concerning nucleation was conducted by Gibbs [12]. In his model, Gibbs suggested that nucleation is a process dominated by two

competing mechanisms: the increase of interface free energy and the reduction of bulk free energy. In the early stage when nuclei are small and the ratio of surface area to bulk is large, interface free energy is dominant. Consequently, small crystal nuclei tend to dissolve spontaneously. Crystal growth becomes energetically favored only after crystal nuclei exceed a critical size.

1.2.1 Classical Nucleation Theory (CNT)

The significance of Gibbs' work is that it offered, for the first time, a quantitative description of nucleation, which could be examined experimentally. After the contribution of Gibbs, further efforts were devoted to developing a more rigorous theoretical foundation of nucleation theory by researchers including Volmer and Webber [13, 14], Farkas [15], Stranski and Kaischew [16] and Becker and Döring [17]. As a result, the so-called classical nucleation theory (CNT) was established in its modern form.

According to CNT, crystal nuclei are nucleated with spherical shape and a structure identical to that of the bulk crystal. Consequently, crystal nuclei share the same physical properties such as surface tension as the bulk crystal. Based on these two assumptions, the change in free energy due to the formation of a crystal nucleus is given by:

$$\Delta G = 4\pi R^2 \gamma + \frac{4}{3}\pi r^3 \frac{1}{\Omega}\Delta\mu \qquad (1\text{-}1)$$

where r is the radius of the nuclei, γ is the surface free energy, Ω is the volume

per molecule and $\Delta\mu$ is the chemical potential difference between the new phase and the mother phase. In a supersaturated system, $\Delta\mu$ is always negative. ΔG reaches its maximum at the critical size r_c in terms of the radius of crystal nuclei. The critical size is determined by setting $d\Delta G / dR = 0$. The expression of r_c is given by:

$$r_c = 2\Omega\gamma / \Delta\mu \tag{1-2}$$

The height of the nucleation barrier can be obtained by substituting Equation (1-2) into Equation (1-1):

$$\Delta G^* = \frac{16\pi\gamma^3\Omega^2}{3\Delta\mu^2} \tag{1-3}$$

The nucleation rate, the number of the newly created critical nuclei per unit time within a unit volume at the steady state, is given by:

$$J = A\exp(-\Delta G^* / k_B T) \tag{1-4}$$

where A is a factor depending on temperature, k_B is Boltzmann's constant.

Equations (1-1)-(1-4) hold only for homogeneous nucleation, that is, when the nucleation occurs spontaneously and randomly without preferential nucleation sites induced by the occurrence of foreign particles. However, in technological applications, crystallization conducted on a substrate plays a key role in developing heterostructures for advanced optics and microelectronics [9, 18-20]. Furthermore, in practice, it is also difficult to remove foreign bodies completely from a crystallizing system. Therefore, in most of the cases of crystallization, we are dealing with heterogeneous nucleation. In heterogeneous nucleation, nuclei form preferentially

near or on the surface of foreign bodies. It is believed that due to the presence of foreign particles, the nucleation barrier will be reduced, and thus nucleation will be enhanced.

To quantify the influence of foreign particles on nucleation, an interfacial correlation functions $f(m,R')$ is introduced [21-24]:

$$f(m,R') = \Delta G^*_{heter} / \Delta G^*_{homo} \tag{1-5}$$

where ΔG^*_{heter} and ΔG^*_{homo} represent the nucleation barrier of heterogeneous and homogeneous nucleation respectively, R' is the ratio of the radius of the foreign body to the radius of the critical nuclei, m is a parameter determined by the interaction between the crystal nuclei and the foreign body as shown in Figure 1.3. $f(m,R') = 1$ means that foreign bodies have no effect in lowering the nucleation barrier, and thus homogeneous nucleation occurs.

1.2.2 Ostwald's rule

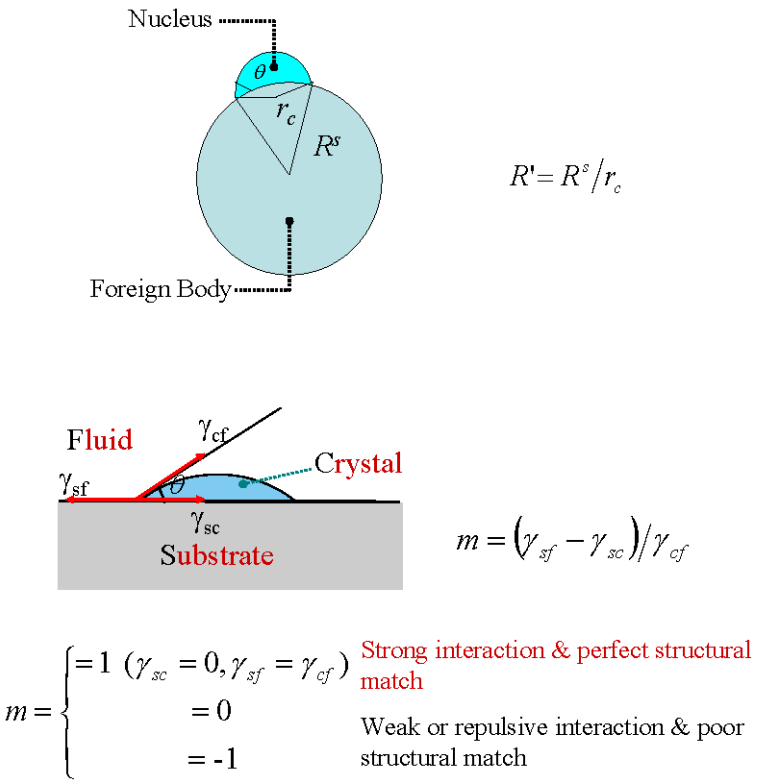

Figure 1.3 Strong interaction between the nucleus and the foreign body can reduce the nucleation barrier and thus enhance the nucleation.

According to CNT, crystal nuclei are formed with identical structure to the final bulk crystal. However, it has long been established that polymorphism, the ability of a molecule to adopt alternative crystal forms, is a widespread and important phenomenon in solid-state chemistry. In a polymorphic system, crystallization may undergo metastable phases before reaching its thermodynamically most stable phase. In polymorphism, the first nucleated crystallites may be distinct in structure to the final crystalline phase, and thus, CNT is not applicable in studying polymorphism.

To interpret polymorphism, Ostwald [25] suggested that the first product of crystallization is not the one that is thermodynamically most stable, but the one that is closest in free energy to the mother phase; this is known as Ostwald's rule.

However, the supersaturation level for the most stable polymorph should be the largest, and then, according to Equations (1-3) and (1-4), the nucleation rate for the most stable polymorph should be the fastest. This implies that the most stable polymorph, contradicting Ostwald's rule, should be expected to first nucleate. An approach to resolve this contradiction is that the surface free energy becomes lower as the phase becomes more metastable. Because the nucleation barrier height is proportional to the square of the surface free energy, a small reduction of surface energy will significantly lower the nucleation barrier, leading to a large increase in nucleation rate. This approach is based on the assumption that the least stable polymorph is the one whose structural organization is most readily derived from the melt or solution, giving rise to the lowest surface energy. This is supported by the discovery of two-step crystallization (TSC) [26-29].

TSC was suggested by ten Wold and Frenkel [26]. According to their study, near the critical point of liquid-liquid phase separation (LLPS), proteins crystallize through a two-step process: as the first step, amorphous dense droplets nucleate from the mother phase through LLPS; subsequently, crystalline nuclei are created from the amorphous dense droplets. In TSC, the amorphous dense droplets are more likely to be first formed from the initial solutions due to their relatively lower surface free

energy with respect to the crystalline structure. Due to its significant implications in science and technology, especially in protein crystallography, TSC has been studied both theoretically [30] and experimentally [31, 32] in the last decade. However, the understanding of TSC has so far remained poor due to the difficulty of directly observing TSC. A major purpose of my studies is to experimentally address the mechanisms underlying TSC

1.3 Crystal Growth

Nucleation forms the initial crystal nuclei which are the basis of the subsequent crystal growth. Precritical nuclei grow or dissolve by chance. Only when a nucleus exceeds a critical size, its growth becomes energetically favorable and thus crystal growth proceeds.

Crystals grow mainly through incorporating adatoms at kink sites. However, it is the way by which adatoms reach kink sites that will eventually determine the properties, such as the quality and surface morphology, of the crystals. The basic way for adatoms to reach kink sites is diffusion on surface and along steps. Another important way is interlayer mass transport which transfers adatoms from upper layers to lower layers; interlayer transport plays a key role in smoothing the growing surfaces. Nucleation of new islands on the existing surfaces is another important process incorporating adatoms into the existing crystals. Nucleation of new islands is likely to occur when the average distance between the existing islands are so large

that an adatoms is very likely to meet another adatom before reaching the existing islands. The equilibrium average distance between islands or mounds on a growing surface is determined by many kinetic factors, such as the surface diffusion rate of adatoms.

Surface diffusion of adatoms is one of the most important kinetic processes underlying crystal growth. The coefficient of surface diffusion is given by [10]:

$$D_{surf} = a^2 \exp(-V_{surf} / k_B T) \tag{1-6}$$

where a is the effective hopping distance between two neighbor sites, V_{surf} is the energy barrier of hopping. Diffusion along steps shows a similar behavior but with a different diffusion energy barrier V_{step}. From Equation (1-6), it is evident that the mobility of adatoms is determined by the diffusion energy barrier and the temperature. High temperature is normally necessary to improve the mobility and thus to produce high-quality crystals.

An important phenomenon in crystal growth is the so-called steering effect. Due to the attraction between the incoming atoms and the growing fronts, incoming adatoms are preferentially absorbed by the uppermost layer of islands, giving rise to a growth instability and rough growing surfaces [33]. To smooth out the islands, interlayer transport transferring adatoms from the upper layers to the lower layers of the islands is critical. Increasing the temperature of the substrate is an effective strategy for improving interlayer transport [34].

Theoretically, to study crystal growth, a group of energy barriers for diffusion and interlayer transport were set up to activate or prohibit the related kinetic processes. Based on these energy barriers, a number of growth models were built [10, 35]. These growth models have been extensively applied in interpreting experimental phenomena; they have thrown new light on our understanding of the process of crystal growth.

1.4 Challenges in the Study of Nucleation and Crystal Growth

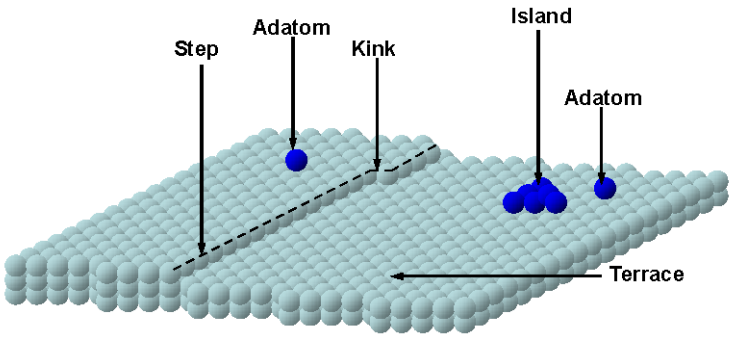

Figure 1.4 Terrace-step-kink (TSK) model of crystal growth.

The purpose of studying crystallization is to obtain a complete understanding of the mechanisms underlying nucleation and crystal growth, which is essential to the exploration of robust experimental strategies of the control of crystal growth. However, although crystallization has been studied experimentally and theoretically for more than a century, a number of fundamental issues of it remain open to question.

Nucleation, the earliest stage of crystallization, plays a critical role in determining

the structure and properties of crystals. Despite its vital role, however, very little is known about nucleation [20, 37]. The main challenge is that the process of nucleation in typical atomic systems is too fast to follow and the size of nuclei is too small for direct observation.

Furthermore, although a number of growth models have been constructed and some of them have succeeded in reproducing experimental observations, many fundamental aspects of crystal growth are still open to question[35, 36] because crystal growth is essentially a result of the interplay between competing kinetic processes and it is difficult theoretically to determine which kinetic process is dominant in a specific growth condition. Experimentally, to determine the dominant mechanisms, direct observation of growth processes is critical.

In science, direct observation of crystallization at the atomic scale is highly desirable in the approach to provide a quantitative understanding of the underlying mechanisms. However, direct observation is very difficult experimentally. The key challenge is that the short length scale and time scale at typical atomic systems make direct observation of nucleation inaccessible to conventional experimental measurements.

By contrast, however, colloidal particles in solutions can be studied directly, because their larger size and much slower time scale makes them experimentally accessible. Most importantly, colloidal particles can serve as good models for atomic or molecular materials, because they exhibit an analogous phase behavior.

1.5 Colloids as a Model for Atomic Systems

Colloid is a system in which solid particles are uniformly dispersed in a medium. The size of solid particles in typical colloids ranges from $1\,nm$ to $1\,\mu m$. Colloids are very common in everyday life, examples including smoke, fog, milk, paint, ink, pigment, aerogel, cheese, butter, glues, etc. Due to their specific properties, suspensions of colloidal particles are of great interest in science and technology.

1.5.1 Properties of Colloids

The most remarkable property of colloidal particles suspended in a fluid is that they exhibit zigzag or random movement, the so-called Brownian motion, which was first observed and studied by Rober Brown in 1827. It is Albert Einstein's work that makes it clear that Brownian motion of colloidal particles in fluids is caused by the thermal motion of the surrounding liquid molecules, and thus Brownian motion offers a visible manifestation of the existence of atoms. Brownian motion of colloidal particles gives rise to osmotic pressure in colloids solutions. Since the osmotic pressure obeys a relationship of the same form as the ideal gas law, colloidal particles in a solution can be viewed as 'big atoms'. In fact, experimental observations have revealed that colloidal suspensions exhibit the same phases, such as gas, liquid and crystal, as observed in typical atomic systems [38, 39].

Because of their ‘atom-like’ properties, colloids have been widely employed as models of atomic systems in studying phase transitions including crystallization [40-42], glass transition [43] and melting [44, 45]. These studies have thrown new light on our understanding of fundamental problems in condensed matter physics.

The major advantage of colloids as a model of atomic systems is that colloidal particles are large enough to be observed directly by microscopy. Furthermore, because of their larger size, the kinetic processes in colloids are much slower and can be followed in real time. These advantages make colloids a useful tool in the study of phase transitions.

1.5.2 Interaction between Colloidal Particles

The phase behavior of colloidal suspensions, similarly to atomic systems, is determined by the nature of the interactions acting between colloidal particles [38]. In practice, interactions between colloidal particles can be adjusted and tuned by adding polymers [46] or applying an external electrical field [41, 47]. The tunable interaction between colloidal particles makes colloid suspensions suitable to model a wide range of systems including protein solutions and atomic systems [38]. In typical colloidal solutions, there are several distinct forces which may affect the behavior of colloids, including electrostatic force, van der Waals force, entropic force and steric force,

Electrostatic force

The colloidal particles in a liquid will become charged by electively absorbing ions or electrons. All the identical colloidal particles take on the same charge (either positive or negative) and thus are repelled by one another. The electrostatic force between colloidal particles is long range and always repulsive.

Van der Waals force

The Van der Waals force is due to interaction between two dipoles which are either permanent or induced. Even if the particles lack a permanent dipole, fluctuations of the electron density gives rise to a temporary dipole in a particle. This temporary dipole induces a dipole in nearby particles. The temporary dipole and the induced dipoles are then attracted to each other. This is known as the Van der Waals force and it is always present. Van der Waals force is short range and attractive.

Entropic force

According to the second law of thermodynamics, a system will spontaneously progress to a state in which entropy is maximized. This can result in effective repulsive forces even between hard spheres.

Steric Force

In a colloid-polymer mixture, steric forces between polymer-covered surfaces or colloidal particles in solutions containing non-adsorbing polymers can modulate

interparticle forces, producing an additional repulsive steric stabilization force or attractive depletion force between them. Experimentally, an effective attractive interaction between two colloidal particles can be induced in a solvent by introducing a smaller polymer molecule, because of the imbalance in osmotic pressure due to depletion of the polymer molecules from the region between the big particles. The range of the attractive interaction is dependent on the size of the polymer, and its strength depends on the polymer concentration [46].

1.5.3 Study of Crystallization in Colloids

In the study of crystallization, because the structure and shape of crystal nuclei have great impact on crystallization, determining the structure and shape of crystal nuclei is of great importance. However, it is a big challenge in atomic systems to visualize and follow a crystal nucleus because of their small size and short time scale. Nevertheless, in a colloidal system, the processes of crystallization can be visualized directly by microscopy. Therefore, the structure and shape of crystal nuclei can be identified experimentally [40]. The study of colloidal crystallization in the last decade has provided a great deal of insight into our understanding of crystallization.

Furthermore, colloidal suspensions with short range attractions share the same phase behavior of protein molecules. Thus, the study of colloidal crystallization is expected to offer insight into protein crystallization which is central to drug design and disease treatment in medicine [48].

Another important motivation of studying the crystallization of colloids is that colloidal crystals have potential applications in fabricating photonic crystals [49, 50]. Therefore, to obtain high-quality colloidal crystals is also technologically important.

Finally, the understanding of the mechanisms of colloid crystallization is also of great importance in exploring robust experimental strategies for controlling self-assembly, which plays a key role in developing advanced materials [51-53].

1.6 Purposes

One of the purposes of this thesis is to study the mechanisms of crystallization, especially of its earliest stage, the so-called nucleation in a two-dimensional colloidal model system. According to CNT, crystal nuclei are identical in structure to the bulk crystal. However, a number of observations have shown that crystal nuclei may undergo a series of metastable structures before they reach the final stable crystalline structure [54-56]. In Chapter 3, the structure of crystal nuclei and its dependence on the size of nuclei will be studied in real space and real time.

An alternative route of crystallization, according to Ostwald's rule, is multi-step crystallization, meaning that a metastable amorphous phase will first form from the mother phase; subsequently, the stable crystalline phase will nucleate from the metastable phase [26]. This kind of mechanism has been studied for many years. However, because of the absence of direct observation, some fundamental aspects of multi-step crystallization remain unclear. In this thesis, multi-step crystallization will

be studied in the colloidal model system which allows a directly observation of the process of crystallization in real space, and thus it enables us to measure some important qualities.

Furthermore, the kinetics underlying crystal growth will be studied at the single-particle level in the colloidal model system. The purpose of the study is to understand the growth instability induced by long-range attractions, which plays a key role in determining the morphology of crystals.

Finally, the real space observation afforded by the colloidal model system enable us to follow the formation of crystal defects in real time and to study their properties including diffusion and the possible configurations.

The studies contained in this thesis are expected to offer insight into our understanding of nucleation and crystal growth. As a possible consequence, the knowledge obtained from these studies may offer some robust experimental strategies for controlling crystallization and self-assembly, which is highly desirable in developing advanced materials.

References

[1] E. Bäuerlein, "Biomineralization of Unicellular Organisms: An Unusual Membrane Biochemistry for the Production of Inorganic Nano- and Microstructures," *Angew. Chem. Int. Ed.*, vol. 42, pp. 614, 2003.

[2] S. Mann, *Biomineralization: Principles and Concepts in Bioinorganic Materials Chemistry*: Oxford University Press, New York, 2001.

[3] C. W. Gouldinga and L. J. Perrya, "Protein production in Escherichia coli for structural studies by X-ray crystallography," *J. Struct. Biol.* , vol. 142, pp. 133, 2003.

[4] A. Pande, J. Pande, N. Asherie, A. Lomakin, O. Ogun, J. King, and G. B. Benedek, "Crystal cataracts: Human genetic cataract caused by protein crystallization," *Proc. Natl. Acad. Sci. USA*, vol. 98, pp. 6116, 2001.

[5] C. A. Ross and M. A. Poirier, "Protein aggregation and neurodegenerative disease," *Nat. Med.*, vol. 10, pp. S10, 2004.

[6] Y. Jia and X. Y. Liu, "Prediction of protein crystallization based on interfacial and diffusion kinetics," *Appl. Phys. Lett.*, vol. 87, pp. 103902 2005.

[7] J. R. Helliwell, "Protein crystal perfection and its application," *Acta. Cryst. D*, vol. 61, pp. 793, 2005.

[8] J. M. Wiencek, "New Strategies for Protein Crystal Growth," *Annu. Rev. Biomed. Eng.*, vol. 01, pp. 505, 1999.

[9] X. Y. Liu and J. J. De Yoreo, "Nanoscale Structure and Assembly at Solid-Fluid Interface," Plenum/Kluwer Academic Publishers, 2004.

[10] Z. Zhang and M. G. Lagally, "Atomistic Processes in the Early Stages of Thin-film Growth," *Science*, vol. 276, pp. 377–383, 1997.

[11] N. Kaiser, "Review of the Fundamentals of Thin-Film Growth," *Appl. Opt.*, vol. 41, pp. 3053, 2002.

[12] J. W. Gibbs, "On the equilibrium of heterogeneous substances," *Trans. Connect. Acad. Sci.* , vol. 16, pp. 343, 1878.

[13] M. Volmer and A. Weber, "Nuclei formation in supersaturated states," *Z. Phys.*

Chem., vol. 119 pp. 277, 1926.

[14] M. Volmer, *Kinetik der Phasenbildung*: Dresden, Leipzig: Steinkopf, Verlag, 1926.

[15] L. Farkas, "Keimbildunggeschwindigkeit in Ubersgttigen Dgmpfen," *Z. Phys. Chem.*, vol. 125, pp. 236, 1927.

[16] I. N. Stranski and R. Kaischew, "Über den mechanismus des gleichgewichtes kleiner kriställchen. I," *Z. Phys. Chem. B*, vol. 26, pp. 100, 1934.

[17] R. Becker and W. Döring, "Kinetische behandlung der keimbildung in ubersattigten damfern," *Ann. Phys.*, vol. 24, pp. 719, 1935.

[18] Z. I. Alferov, "The history and future of semiconductor heterostructures," *Semiconductors*, vol. 32, pp. 1, 1998.

[19] V. A. Shchukin and D. Bimberg, "Spontaneous ordering of nanostructures on crystal surfaces," *Rev. Mod. Phys.*, vol. 71, pp. 1125, 1999.

[20] X. Y. Liu, "From molecular structure of solid-fluid interfaces to nucleation kinetics: implications for nanostructure engineering," in *Nanoscale structure and assembly at solid-fluid interfaces*, X. Y. Liu and J. J. De Yoreo, Eds.: Plenum/Kluwer Academic Publisher, 2004.

[21] X. Y. Liu, "Generic mechanism of heterogeneous nucleation and molecular interfacial effects," in *Advances in Crystal Growth Research*, K. Sato, K. Nakajima, and Y. Furukawa, Eds.: ELSEVIER SCIENCE B.V., Amsterdam, 2001, pp. 42.

[22] X. Y. Liu, "Generic progressive heterogeneous processes in nucleation," *Langmuir*, vol. 16, pp. 7337, 2000.

[23] X. Y. Liu, "A new kinetic model for 3D heterogeneous nucleation," *J. Chem. Phys.* , vol. 111, pp. 1628, 1999.

[24] X. Y. Liu, K. Maiwa, and K. Tsukamoto, "Two-dimensional heterogeneous nucleation and the growth kinetics," *J. Chem. Phys.* , vol. 106, pp. 1870, 1997.

[25] W. Ostwald, "Studien über die Bildung und Umwandlung fester Körper," *Z. Phys. Chem.* , vol. 22, pp. 289, 1897.

[26] P. R. ten Wolde and D. Frenkel, "Enhancement of Protein Crystal Nucleation by Critical Density Fluctuations," *Science*, vol. 277, pp. 1975-1978, 1997.

[27] P. R. ten Wolde and D. Frenkel, "Homogeneous nucleation and the Ostwald step rule," *Phys. Chem. Chem. Phys.*, vol. 1, pp. 2191, 1999.

[28] X. Chen, A. C. S. Samia, Y. Lou, and C. Burda, "Investigation of the Crystallization Process in 2 nm CdSe Quantum Dots," *J. Am. Chem. Soc.*, vol. 127, pp. 4372-4375, 2005.

[29] J. F. Lutsko and G. Nicolis, "Theoretical Evidence for a Dense Fluid Precursor to Crystallization," *Phys. Rev. Lett.*, vol. 96, pp. 046102, 2006.

[30] L. Addadi and S. Weiner, "Control and Design Principles in Biological Mineralization," *Angew. Chem. Int. Ed. Engl.* , vol. 31, pp. 153 1992.

[31] E. Beniash, J. Aizenberg, L. Addadi, and S. Weiner, "Amorphous calcium carbonate transforms into calcite during sea urchin larval spicule growth," *Proc. R. Soc. London Ser. B*, vol. 264, pp. 461, 1997.

[32] L. Addadi, S. Raz, and S. Weiner, "Taking Advantage of Disorder: Amorphous Calcium Carbonate and Its Roles in Biomineralization," *Adv. Mater.* , vol. 15, pp. 959, 2003.

[33] J. Seo, -. M. Kwon, H.-Y. Kim , and J.-S. Kim, "Steering effect on the shape of islands for homoepitaxial growth of Cu on Cu (001)," vol. 67, pp. 121402, 2003.

[34] F. Montalenti, M. R. Sørensen, and A. F. Voter, "Closing the Gap between Experiment and Theory: Crystal Growth by Temperature Accelerated Dynamics," *Phys. Rev. Lett.* , vol. 87, pp. 126101, 2001.

[35] H. Jónsson, "Theoretical Studies of Atomic-Scale Processes Relevant to Crystal Growth," *Annu. Rev. Phys. Chem.*, vol. 51, pp. 623, 2000.

[36] S. C. Wang and G. Ehrlich, "Atom Incorporation at Edge Defects in Clusters," *Phys. Rev. Lett.*, vol. 93, pp. 176101, 2004.

[37] X. Y. Liu, "Heterogeneous nucleation or homogeneous nucleation?," *J. Chem. Phys.* , vol. 112, pp. 9949, 2000.

[38] V. J. Anderson and H. N. W. Lekkerkerker, "Insights into phase transition

kinetics from colloid science," *Nature*, vol. 416, pp. 811, 2002.

[39] D. Frenkel, "Playing Tricks with Designer “Atoms”," *Science*, vol. 296, pp. 65, 2002.

[40] U. Gasser, E. R. Weeks, A. SchoÞeld, P. N. Pusey, and D. A. Weitz, "Real-Space Imaging of Nucleation and Growth in Colloidal Crystallization," *Science*, vol. 292, pp. 258, 2001.

[41] K.-Q. Zhang and X. Y. Liu, "In situ observation of colloidal monolayer nucleation driven by an alternating electric field," *Nature*, vol. 429, pp. 739, 2004.

[42] Y. Liu, J. Narayanan, and X. Y. Liu, "Colloidal Phase Transition Driven by Alternating Electric Field," *J. Chem. Phys.* , vol. 124, pp. 124906, 2006.

[43] S. Manley, H. M. Wyss, K. Miyazaki, J. C. Conrad, V. Trappe, L. J. Kaufman, D. R. Reichman, and D. A. Weitz, "Glasslike Arrest in Spinodal Decomposition as a Route to Colloidal Gelation," *Phys. Rev. Lett.*, vol. 95, pp. 238302, 2005.

[44] A. M. Alsayed, M. F. Islam, J. Zhang, P. J. Collings, and A. G. Yodh, "Premelting at Defects Within Bulk Colloidal Crystals," *Science*, vol. 309, pp. 1207, 2005.

[45] K.-Q. Zhang and X. Y. Liu, "Two Scenarios for Colloidal Phase Transitions," *Phys. Rev. Lett.* , vol. 96, pp. 105701, 2006.

[46] W. C. K. Poon, "The physics of a model colloid–polymer mixture," *J. Phys: Condens Matter Chem. B*, vol. 14, pp. R859, 2002.

[47] A. Yethiraj and A. v. Blaaderen, "A colloidal model system with an interaction tunable from hard sphere to soft and dipolar," *Nature*, vol. 421, pp. 513, 2003.

[48] I. Tickle, A. Sharff, M. Vinković, J. Yon, and H. Jhoti, "High-throughput protein crystallography and drug discovery," *Chem. Soc. Rev.* , vol. 33, pp. 558, 2004.

[49] E. Istrate and E. H. Sargent, "Photonic crystal heterostructures and interfaces," *Rev. Mod. Phys.*, vol. 78, pp. 455, 2006.

[50] Y. Wang, M. Ibisate, Z.-Y. Li, and Y. Xia, "Metallodielectric Photonic Crystals

Assembled from Monodisperse Spherical Colloids of Bismuth and Lead," *Adv. Mater.* , vol. 18, pp. 471, 2006.

[51] G. M. Whitesides and M. Boncheva, "Beyond molecules: Self-assembly of mesoscopic and macroscopic components" *Proc. Natl. Acad. Sci. USA*, vol. 99, pp. 4769, 2002.

[52] G. M. Whitesides and B. Grzybowski, "Self-Assembly at All Scales," *Science*, vol. 295, pp. 2418, 2002.

[53] H. Yusuf, W.-G. Kim, D. H. Lee, M. Aloshyna, A. G. Brolo, and M. G. Moffitt, "A Hierarchical Self-Assembly Route to Three-Dimensional Polymer-Quantum Dot Photonic Arrays," *Langmuir*, vol. 23, pp. 5251, 2007.

[54] D. Moroni, P. R. ten Wolde, and P. G. Bolhuis, "Interplay between Structure and Size in a Critical Crystal Nucleus," *Phys. Rev. Lett.*, vol. 94, pp. 235703, 2005.

[55] J. Anwar and P. K. Boateng, "Computer Simulation of Crystallization from Solution," *J. Am. Chem. Soc.*, vol. 120, pp. 9600, 1998.

[56] A. Lomakin, N. Asherie, and G. B. Benedek, "Liquid-Solid Transition in Nuclei of Protein Crystals," *Proc. Natl. Acad. Sci. USA*, vol. 100, pp. 10254, 2003.

Chapter 2 Experimental Techniques and Analysis Methods

2.1 Experimental Techniques

Figure 2.1 shows the experimental setup. Monodisperse colloidal particles (polystyrene spheres of diameter 0.99 μm, polydispersity < 5%, Bangs Laboratories) were dispersed uniformly in deionized water. The colloidal suspension was then sealed between two parallel horizontal conducting glass plates coated with indium tin oxide (ITO). In this system, fluid flows induced by an alternating electric field (AEF) transport the colloidal particles to the surface of the glass plates where two-dimensional crystals are formed under certain conditions. The processes of crystallization were recorded for analysis by a digital camera (CoolSNAP cf, Photometrics) which was mounted on an Olympus BX51 microscope.

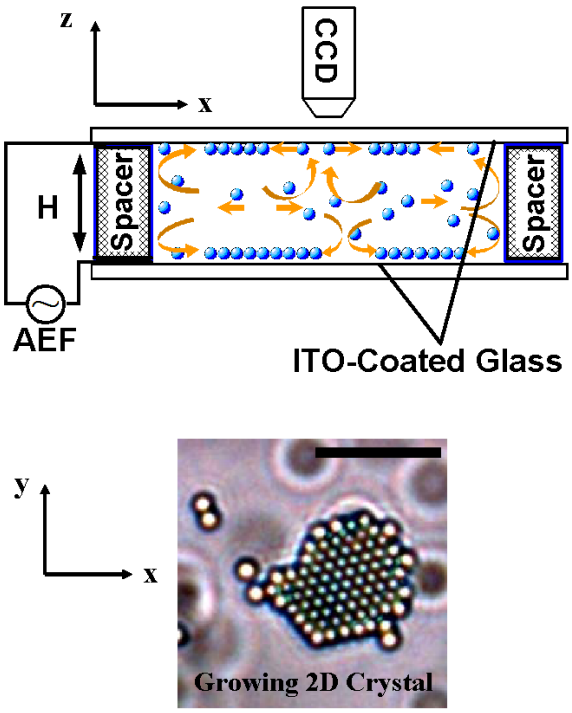

Figure 2.1 Experimental setup: colloidal suspension is sealed between two pieces of ITO-coated conducting glass plates separated by insulating spacers. The gap between the two glass plates is $H = 120 \pm 5\ \mu m$. The dynamic process is recorded by a digital camera for analysis. Scale bar: 10 μ m.

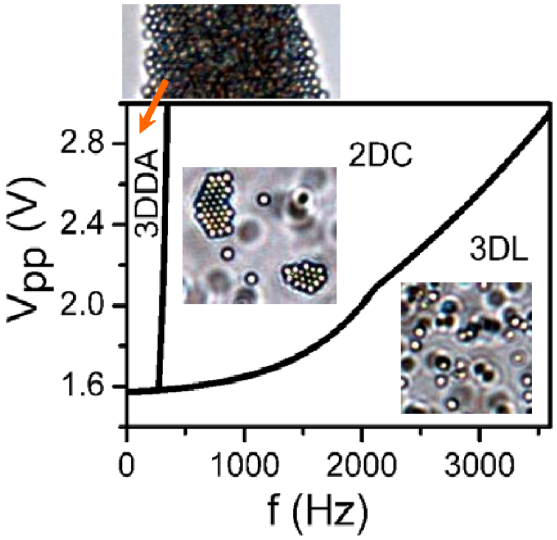

Figure 2.2 Phase diagram: three phases are identified in our experiments: two-dimensional crystal phase (2DC), three-dimensional liquid phase (3DL) and three-dimensional disordered aggregation (3DDA). Solid volume fraction: 0.03%. Na_2SO_4 : 10^{-4} M.

2.2 Experimental Phenomena

In this system, the phase diagram is determined by the solid volume fraction and the interaction acting between colloidal particles. In our experiments, the effective interaction between colloidal particles is modified by adding salt Na_2SO_4. There are three possible phases in this system: two-dimensional crystal phase (2DC), three-dimensional liquid phase (3DL) and three-dimensional disordered aggregation (3DDA). Changing the solid volume fraction and the salt concentration will shift the phase boundaries on the frequency (f)-voltage (V) plane, giving rise to a change of the location and size of the windows for 2DC, 3DL and 3DDA.

Figure 2.2 shows the phase diagram of the solution with solid volume fraction ϕ=0.03% and salt concentration 10^{-4} M.

2.3 Attractive Forces between Colloidal Particles

Colloidal particles in our system are negatively charged and thus repel each other. However, when an AEF is applied to the suspension, colloidal particles are transported to the surfaces of the glass plates by fluid flows induced by the AEF. In this system, a long-range attractive force between the colloidal particles is induced by an electrohydrodynamic (EHD) mechanism [1, 2], giving rise to the aggregation of colloidal particles. The underlying mechanism of the long-range attraction is that the presence of a charged particle near the electrode surface distorts the local electric field, and thus leads to a gradient in local current density, generating a localized fluid flow

that carries the particles towards each other.

Both the quantitative theoretical model and the experimental investigation suggested that there exists a critical frequency below which the long-range attractive force dominates the particle-particle interaction and leads to the aggregation of the particles, while above the critical frequency the repulsive Columbic and dipole-dipole interactions become dominant, and then no aggregation occurs. This explains why crystallization or aggregation can occur only below a certain frequency at a specific strength of the electric field as shown in Figure 2.2. The quantitative analysis of the EHD flow velocity suggests that the long-range attraction scales with the square of the applied electric field strength and inversely with frequency.

2.4 Image Processing

To analyze the structure of the crystal nuclei and track an individual particle from the series of pictures, it is necessary to identify the location of a colloidal particle in a colloidal cluster. To achieve this purpose, an image processing program is developed in house to extract the locations of colloidal particles from a picture.

As can be seen in Figure 2.3(a), colloidal particles in the experimental images are represented by bright spots. In image processing, all neighbor pixels with brightness higher than a critical user-defined threshold are grouped into a cluster. The center of mass of the cluster is determined and taken as the location of the colloidal particle. As an example of image processing, the locations of the colloidal particles in Figure 2.3(a)

are identified by our image processing program. The locations are replotted in Figure 2.3(b) in which each site (dot) corresponds to a colloidal particle and the lines connecting sites represent the nearest-neighbor bonds. .

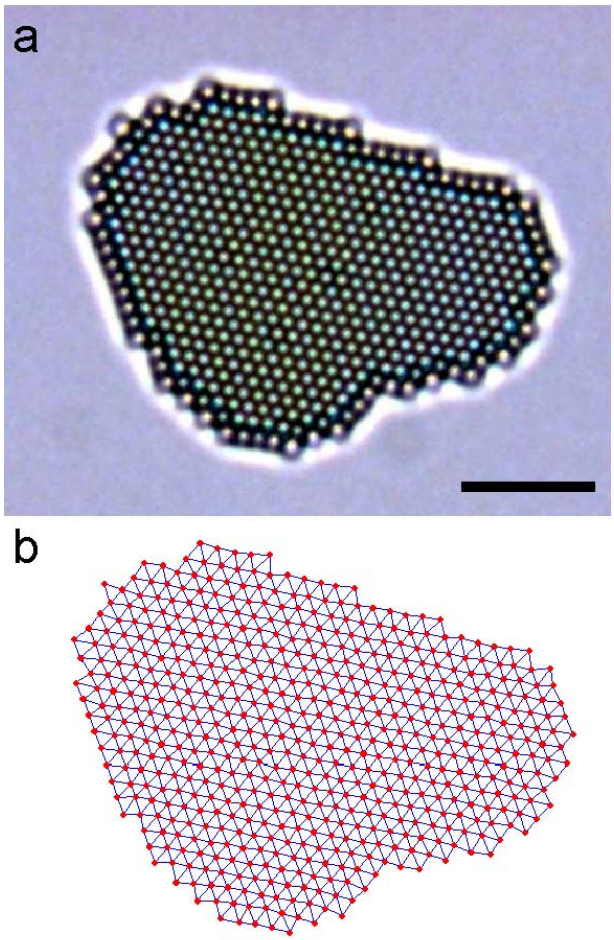

Figure 2.3 Result of imaging processing: (a) A 2D crystal obtained from experiment. (b) Positions (dots) of colloidal particles obtained from image processing. Scale bar: 10 μ m.

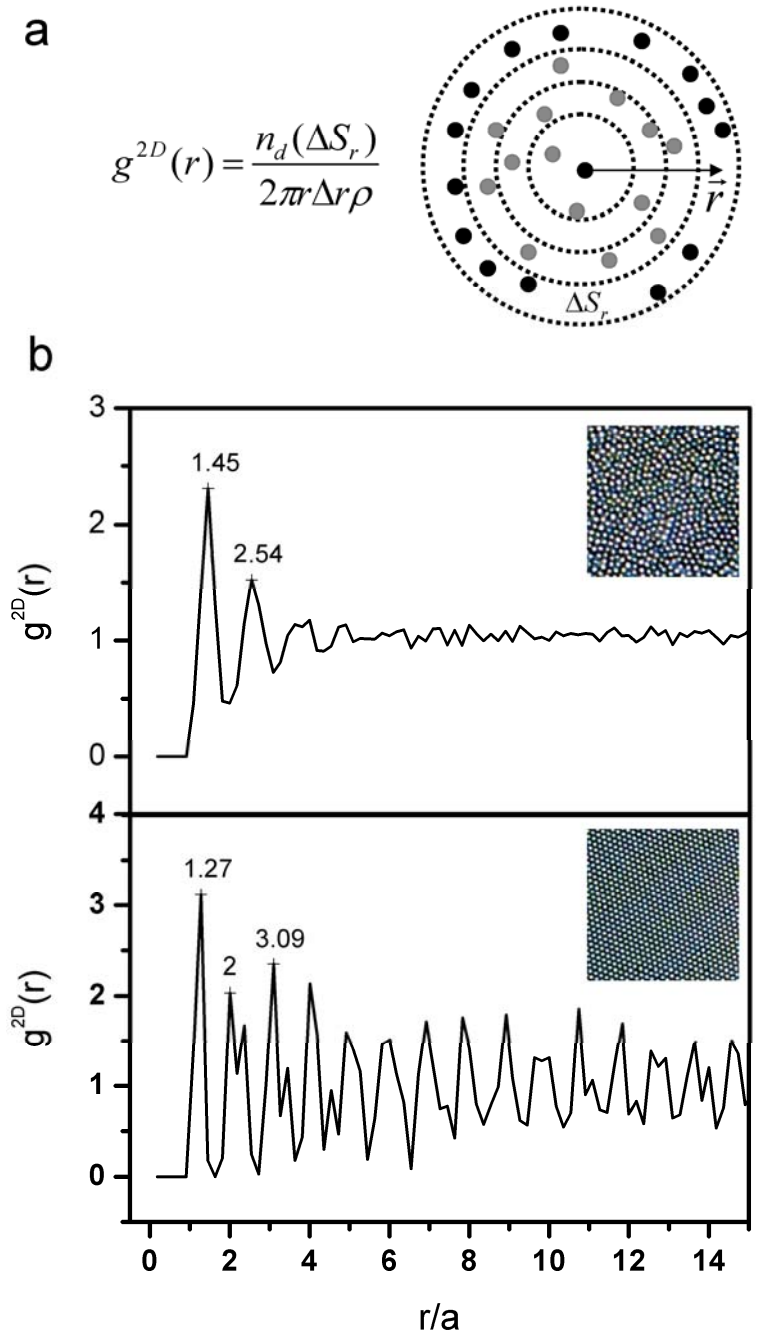

Figure 2.4 2D radial pair correlation functions: (a) Definition of 2D radial pair correlation function. (b) 2D radial pair correlation functions of liquid-like colloidal clusters and 2D hexagonal lattice. a is the diameter of the colloidal particles.

2.5 Order Parameters

To quantify the structure of a colloidal cluster, it is necessary to define some order parameters to determine the order degree of the colloidal clusters. In this study, a two-dimensional pair correlation function $g^{2D}(r)$ and a local bond-order parameter $\psi_6(r)$ are employed.

2.5.1. Pair Correlation Function

The most often used order parameter is the pair correlation function, which is defined as [4]:

$$G(\vec{r}) = \frac{1}{N}\sum_{j=1}^{N}\sum_{i=1}^{N} < \delta(\vec{r} - (\vec{r}_j - \vec{r}_i)) > \qquad (2\text{-}1)$$

where N is the number of particles, $\vec{r}_j$ and $\vec{r}_i$ are the coordinates of particles i and j, respectively. $\delta(\vec{r})$ is the delta function. In practice, the radial pair correlation function is more frequently used rather than the pair correlation function. The 2D radial pair correlation function $g^{2D}(r)$ is given by:

$$g^{2D}(r) = \frac{n_d(\Delta S_r)}{2\pi r \Delta r \rho} \qquad (2\text{-}2)$$

Where ρ is the average particle density, ΔS_r is the area of a ring with an inner radius of $r - \Delta r/2$ and an outer radius of $r + \Delta r/2$ (Figure 2.4(a)). $n_d(\Delta S_r)$ is the mean number of particles found in the ring, given that there is a particle at $\vec{r} = 0$. The top curve of Figure 2.4(b) is a 2D radial pair correlation function for a disordered or liquid-like colloidal cluster obtained in our experiments; the bottom curve of Figure

2.4(b) gives the 2D radial pair correlation function of a 2D hexagonal crystal. The height of the peaks of $g^{2D}(r)$ corresponds to the strength of the correlation. The value 1 of $g^{2D}(r)$ means no correlation. For a liquid-like structure as can be seen from the top curve of Figure 2.4(b), the envelope of $g^{2D}(r)$ decays to unity within a few diameters, suggesting that the correlation is short-range. However, the envelope of $g^{2D}(r)$ for a typical hexagonal crystal, as the bottom curve of Figure 2.4(b) shows, remain fluctuating around 1 even as the distance is much larger 10. It means that the correlation in a crystal is long-range. Therefore, in practice the decay length of $g^{2D}(r)$ is often used as a quantitative description of order degree. The position of the first peak of $g^{2D}(r)$ corresponds to the average center-to-center distance between a colloidal particle and its nearest neighbors.

2.5.2 Local Bond-Order Parameter

The radial pair correlation function is a global order parameter to examine the order degree of a colloidal cluster. The ability to detect crystalline regions from the growing liquid-like clusters is critical in studying multi-step crystallization. To achieve this, a local 2D bond-order parameter is employed in our study, which is defined as:

$$\psi_6(r_i) = \frac{1}{N} \left| \sum_{j=1,N} \exp(-i6\theta_{ij}) \right| \qquad (2\text{-}3)$$

where r_i is the center of particle i, and θ_{ij} is the angle subtended between the vector from particle i to its jth nearest neighbor and the arbitrarily chosen x axis. N is the

number of nearest neighbors of particle *i*. The mean value $<\psi_6(r_i)>$ for a typical liquid-like cluster in our experiments is 0.50. For a typical crystal, $<\psi_6(r_i)>$ is measured as 0.80 which is taken as one of the criterions for crystal-like particles in our studies. However, since liquid has short-range order, it is highly desirable to find some particles with $\psi_6(r_i) \geq 0.8$ in a liquid-like cluster. Therefore, single particles with $\psi_6(r_i) \geq 0.8$ will not be considered as a real crystal-like particle. In our studies, a domain, in which all particles are characterized by $\psi_6(r_i) \geq 0.8$, will be considered as a crystalline nucleus if it contains at least one particle which has no a nearest neighbor with $\psi_6(r_i) < 0.8$. Only particles belonging to a crystalline nucleus will be considered as crystal-like particles. On the other hand, it is also normal in a crystalline nucleus to find some particles with $\psi_6(r_i) < 0.8$. These particles will be considered as crystal defects and are also counted as crystal-like particles.

Figure 2.6(a) shows a cluster obtained from our experiments. In this cluster, all particles with $\psi_6(r_i) \geq 0.8$ is identified and represented by solid circles in Fig. 2.6(b). However, only part of these particles will be considered as crystal-like particles as indicated above. The particles which are considered as real crystal-like particles are shown by solid circles in Fig. 2.6(c). In Fig. 2.6(c), the cluster is divided into two regions: crystal and liquid. The interface between these two regions is defined as the crystal-liquid boundary.

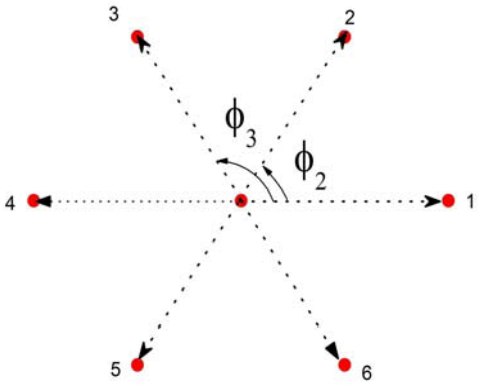

$$\psi_6 = \frac{1}{N} \left| \sum_{i=1,N} \exp(-i6\phi_i) \right|$$

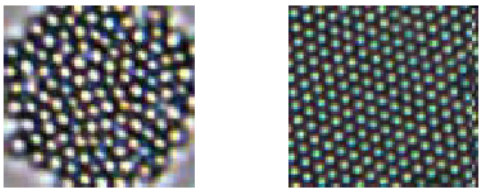

$\langle \psi_6 \rangle = 0.50$ $\langle \psi_6 \rangle = 0.80$

Figure 2.5 2D bond-order parameter

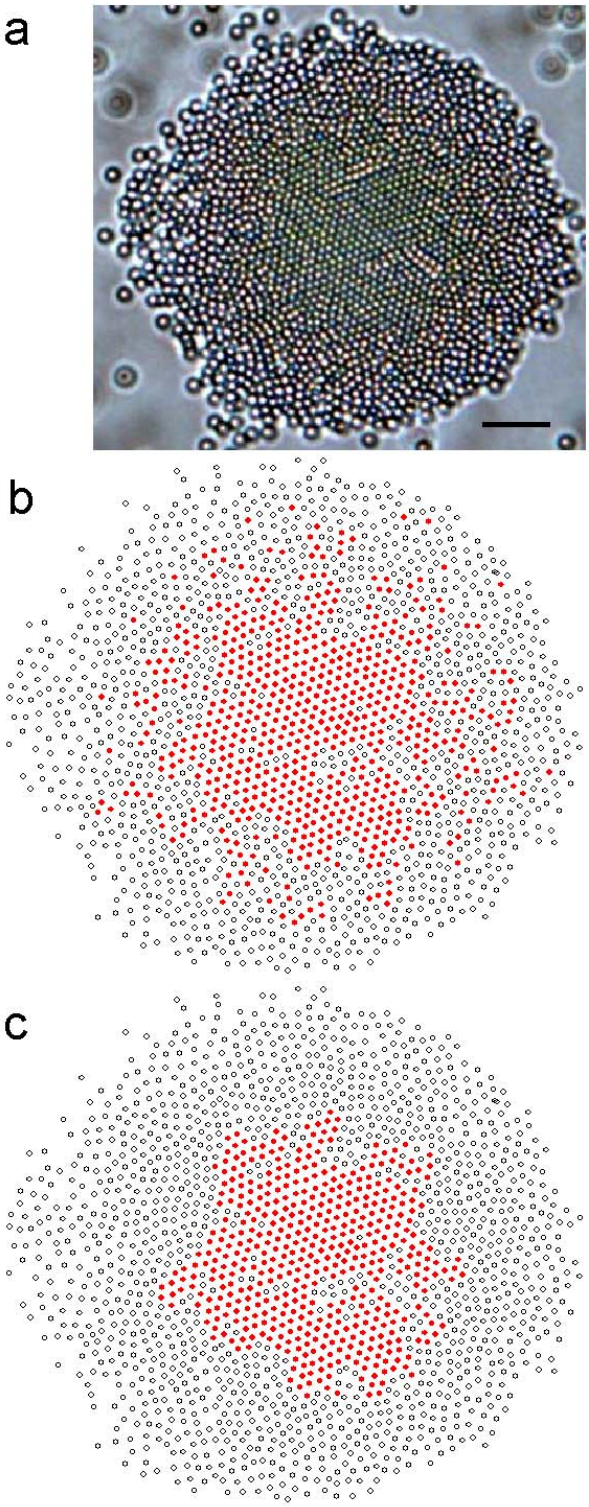

Figure 2.6 Identification of crystal-like particles. (a) Original figure from experiments. (b) Particles with the bond-order parameter larger or equal to 0.8 are identified and represented by solid circle. (c) Crystal-like particles (solid circle). Scale bar: 10μm.

References

[1] S.-R. Yeh, M. Seul, and B. I. Shraiman, "Assembly of ordered colloidal aggregrates by electric-field-induced fluid flow," *Nature* vol. 386, pp. 57, 1997.

[2] M. Trau, D. A. Saville, and I. A. Aksay, "Assembly of colloidal crystals at electrode interfaces," *Langmuir*, vol. 13, pp. 6375, 1997.

[3] F. Nadal, F. Argoul, P. Hanusse, B. Pouligny, and A. Ajdari, "Electrically induced interactions between colloidal particles in the vicinity of a conducting plane," *Phys. Rev. E*, vol. 65, pp. 061409, 2002.

[4] J. Bongers, H. Manteufel, H. Versmold, and K. Vondermaßen, "Microscopic measurements of correlation functions in colloid dispersions," *J. Chem. Phys.*, vol. 108, pp. 9937, 1998.

Chapter 3 Size Dependence of the Structure of Nuclei

3. 1 Introduction

According to classical nucleation theory (CNT) [1, 2], crystal nuclei arise from thermal fluctuations. Due to the competition between the increased surface free energy and the reduced bulk free energy, the growth of crystal nuclei has to overcome an energy barrier. Consequently, crystal nuclei need to reach a critical size before their growth becomes energetically favorable. The quantitative description of the critical size and nucleation barrier is given by Equations (1-2) and (1-3). Equations (1-2) and (1-3) are derived with assumptions that the structure and surface tension of the crystal nuclei are identical to those of the bulk crystal.

Theoretically, however, it has also been argued that when critical nuclei are small, due to the large ratio of the surface to the volume, the properties of the crystal nuclei

are dominated by surface effects. Consequently, it is very likely for the nuclei to adopt a liquid-like structure at their earliest stage of formation [3]. This argument was supported by simulations [4, 5]. According to the simulations, crystal nuclei nucleate with metastable structures different from that of the bulk crystal, and experience a structure transition in the subsequent growth. However, due to the difficulty of directly observing the nucleation process, the kinetics of this sort of structure transition has so far not been studied experimentally.

In this chapter, we study the size dependence of the structure of crystal nuclei in the two-dimensional colloidal system by means of real space and real time observation. The mechanism and consequences of the presence of the metastable structures are discussed. In this study, the concentration of Na_2SO_4 is 2×10^{-4} M.

3. 2 Structure of Precritical Nuclei

Figure 3.1(a)-(c) show a snapshot sequence of the growth of crystal nuclei under conditions V_{pp}=2.5 V and f=5000 Hz. Initially, the structure of the nucleus is essentially disordered (Figure 3.1(a)). As it grows, its core becomes ordered gradually (Figure 3.1(b)). The nucleus becomes entirely ordered when it contains more than 90 particles (Figure 3.1(c)). In this process, it is clear that the structure of the nucleus is size dependent, that is, the growth of the nucleus involves not only an increase in size but also a rise in the degree of crystallinity. To quantify the size dependence of the degree of crystallinity, the average bond-order parameter $<\psi_6>$ of the nucleus is

measured as a function of the nucleus size. In Figure 3.2, both $<\psi_6>$ and the nucleus size N are plotted as a function of time. It can be seen that as the size increases with time, $<\psi_6>$ increases gradually. However, to become entirely ordered, the crystal nuclei have to grow beyond a critical size. To determine the critical size, $<\psi_6>$ is fit as a function of time. The corresponding size at which the fitting curve reaches 0.8 is defined as the critical size beyond which nuclei becomes entirely ordered. This critical size is denoted hereafter as the structure transition size N_{trans}. Under conditions of V_{pp}=2.5 V and f=5000 Hz, N_{trans} is measured at ~80 as shown in Figure 3.2.

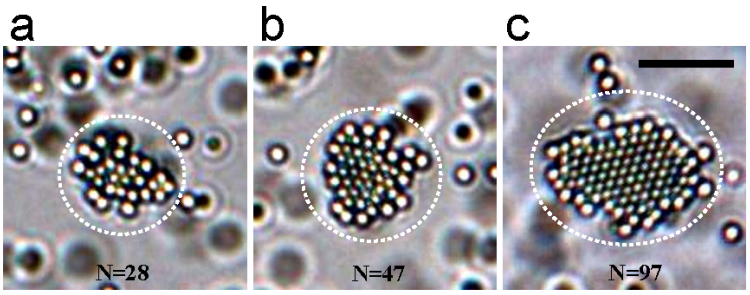

Figure 3.1 The structure of precritical nuclei is dependent on their size. (a) The initial structure of a crystal nucleus is liquid-like due to surface effects. (b) The crystal nucleus develops a crystalline core when it gets big enough. (c) The crystal nucleus has an entirely crystalline structure when it grows beyond a critical size. Scale bar: 10 μm

The occurrence of the metastable liquid-like structure as shown in Figure 3.1 is in contrast with the prediction of CNT. However, nucleation of crystal nuclei via metastable structures had been observed in simulations before this study. For example, the structure of precritical nuclei was found to be body-centered cubic (BCC) which subsequently transforms to the more stable face-centered cubic (FCC) [6]. Recent simulations [3, 4] revealed that a liquid-like structure is favored by small nuclei, and

entirely crystalline structures are possible only when the number of nuclei exceeds a certain value. In these studies, the structure transition from liquid-like to crystal-like occurs sharply at a critical size. However, in our experiments as described above, the transition is a continuous process.

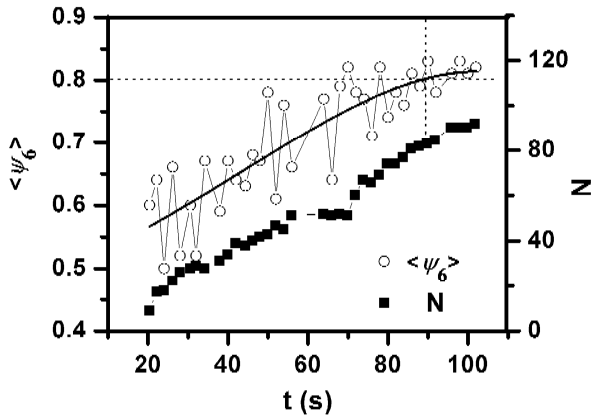

Figure 3.2 The order degree of crystal nuclei increases gradually with the size. The nuclei become entirely crystalline when the size exceeds a critical value. The critical size is determined as ~80 under conditions 5000 Hz and 2.5 V.

3. 3 Effect of the Liquid-Like Exterior on Nucleation

Nucleation is a thermodynamic process. Thus, the route adopted by nucleation should be thermodynamically favored. To identify the mechanism underlying the continuous structure evolution as shown in Figure 3.1, let us consider a nucleus, its free energy is given by:

$$G = n_s \alpha + n_b \mu \tag{3-1}$$

Free energy of a nucleus consists of two part: surface free energy $n_s \alpha$, where n_s is the number of surface particles, α is the surface free energy per surface particle;

bulk free energy $n_b\mu$, where n_b is the number of bulk particles, μ is the chemical potential of a bulk particle. The free energy difference between a liquid-like nucleus and a crystal-like nucleus is given by:

$$\Delta G_{CL} = G_C - G_L = n_s(\alpha_C - \alpha_L) - n_b(\mu_L - \mu_C) \tag{3-2}$$

L and *C* denote the liquid-like and crystal-like nucleus, respectively. In a crystallizing system, one should have: $\mu_L > \mu_C$ and $\alpha_L < \alpha_C$. It was found that $\alpha_C - \alpha_L$ is normally several times larger than $\mu_L - \mu_C$, because the entropy of a surface liquid-like particle is much larger than that of a bulk liquid-like particle, while the entropy difference between a surface and a bulk crystal-like particle is slight [3]. Therefore, for small nuclei with $n_s > n_b$, $\Delta G_{CL} < 0$ persists, suggesting that a liquid-like structure is more favorable in energy than the crystal-like structure for a nucleus consisting of mainly surface particles. Only when the nuclei contain enough bulk particles and $\Delta G_{CL} < 0$, can the crystal-like structure become energetically favorable. The size defined by $\Delta G_{CL} = 0$ corresponds to the critical size at which the transition from the liquid-like structure to the crystal-like structure occurs. Given $\Delta G_{CL} = 0$, it follows that:

$$\frac{n_b^*}{n_s^*} = \frac{\alpha_C - \alpha_L}{\mu_L - \mu_C} \tag{3-3}$$

The transition size N_{trans} is given by $n_b^* + n_s^*$, where n_b^* and n_s^* are the numbers of bulk particles and surface particles, respectively contained in nuclei of the transition size. Below N_{trans}, liquid-like structure is favored by nuclei. At N_{trans}, an addition of a few or even one particle to the liquid-like nucleus will induce a global

structure transition. This sort of sharp transition in structure is the picture delivered by Lomakin et al [3]. However, in our experiments, the evolution of the structure of the nucleus as seen from Figures 3.1 and 3.2 is a continuous process, with the crystal-like component increasing gradually in the core of the nucleus while the liquid-like component is maintained in the exterior layer. In this case, the free energy of the nuclei should be expressed as:

$$G_L = n_s \alpha_L + n_b \mu_C \tag{3-4}$$

Since $\mu_L > \mu_C$, it is clear that energetically, a nucleus with a crystal-like core and a liquid-like exterior has a lower free energy than an entirely liquid-like nucleus. This may explain why a continuous instead of a sharp structure transition is adopted in our experiments: the crystal-like core contributes a lower bulk free energy while the liquid-like exterior layer contributes a lower surface free energy.

According to CNT, crystal nuclei have the same structure as that of the bulk crystal. However, due to the competition between the surface effects and the bulk properties, there exist a nucleation energy barrier and thus a critical size for crystal nuclei. Below the critical size, the properties of nuclei are dominated by surface effects, and thus they tend to shrink or dissolve. Nuclei have to be larger than the critical size before their growth becomes energetically favored. Similarly in our experiments, the growth of an entirely crystal-like nucleus becomes energetically favorable only when they exceed the structure transition size N_{trans}. Accordingly, we conclude that the transition size in our experiments is physically equivalent to the

critical size defined by CNT.

According to two-dimensional (2D) CNT [7, 8], the change of free energy induced by the formation of a 2D crystal nucleus is given by:

$$\Delta G = -\frac{\pi r^2}{A}\Delta\mu_c + 2\pi r\gamma_c \tag{3-5}$$

where r is the radius of the nucleus, A is the area per structure unit, $\Delta\mu_c$ is the chemical potential change of transforming a growth unit from the mother phase to the crystalline phase, γ_c is the line tension of 2D crystals. The 2D critical size r_c is obtained by setting $d(\Delta G)/dr = 0$:

$$r_c = \frac{\gamma_c A}{\Delta\mu_c} \tag{3-6}$$

and correspondingly, the nucleation barrier is:

$$\Delta G_{crit} = \frac{\pi\gamma_c^2 A}{\Delta\mu_c} \tag{3-7}$$

However, our experiments show that sub crystal nuclei are normally covered by a liquid-like exterior layer as shown in Figure 3.1(a) and (b) before they reach the transition size. In this case, the line tension of 2D crystals in Equation (3-7) should be replaced by that of 2D liquid droplets, and then the critical size should be given by:

$$r_c^* = \frac{\gamma_L A}{\Delta\mu_c} \tag{3-8}$$

The corresponding nucleation barrier is thus given by:

$$\Delta G_{crit}^* = \frac{\pi\gamma_L^2 A}{\Delta\mu_c} \tag{3-9}$$

Comparing Equation (3-6) and Equation (3-8), it is found that since $\gamma_L < \gamma_c$, the critical size of the crystal nuclei is smaller than what was predicted by CNT due to

the presence of the liquid-like exterior layer, Consequently, the nucleation barrier is also reduced: $\Delta G^*_{crit} < \Delta G_{crit}$. The reduced nucleation barrier ΔG^*_{crit} is related to the CNT-predicted ΔG_{crit} by:

$$\Delta G^*_{crit} = (\frac{\gamma_L}{\gamma_c})^2 \Delta G_{crit} \tag{3-10}$$

3. 4 Transient Crystalline Structure at High Supersaturations

Figure 3.3 shows a typical growth process of nuclei observed at *f*=3000 Hz and V_{pp} =2.5 V. Figure 3.3(a) shows that from time to time, $< \psi_6 >$ jumps from 0.6 to 0.8, through fluctuation even before it reaches its transition size (~30). This suggests that the nucleus undergoes global structure transition between liquid-like and crystal-like from time to time as shown by Fig. 3.3(b)-(e). This sort of structural transition is attributed to the reduction of the energy barrier between the metastable liquid-like structure and the stable crystalline structure.

In our system, a decreasing of frequency gives rise to the increase of the supersaturation necessary for crystallization. According to Equation (3-7), the increase of supersaturation will reduce nucleation barrier. Thus one should expect that at high enough supersaturations, the nucleation barriers of all possible structures are so low that the energy barrier between the metastable liquid-like structure and the stable crystal-like structure may be lower than $k_B T$. In this case, thermal fluctuations may induce a transformation from the liquid-like structure to the crystal-like structure or vice versa as illustrated by Fig. 3.3(b)-(e).

A common feature in Figures 3.2 and 3.3(a) is the fluctuation of $<\psi_6>$. The fluctuation magnitude of $<\psi_6>$ at the high supersaturation (Fig. 3.3(a), *f*=3000Hz) is around 0.20 while it is around 0.15 at a lower supersaturation (Fig. 3.2, *f*=5000Hz). The higher fluctuation of $<\psi_6>$ at the higher supersaturation is because that the energy barrier between the precritical nuclei a metastable liquid-like structure and the precritical nuclei with a stable crystal-like structure is reduced by increasing supersaturation. Therefore, with the same magnitude of thermal fluctuation, precritical nuclei at high supersaturations can reach a structure with a higher ordering degree.

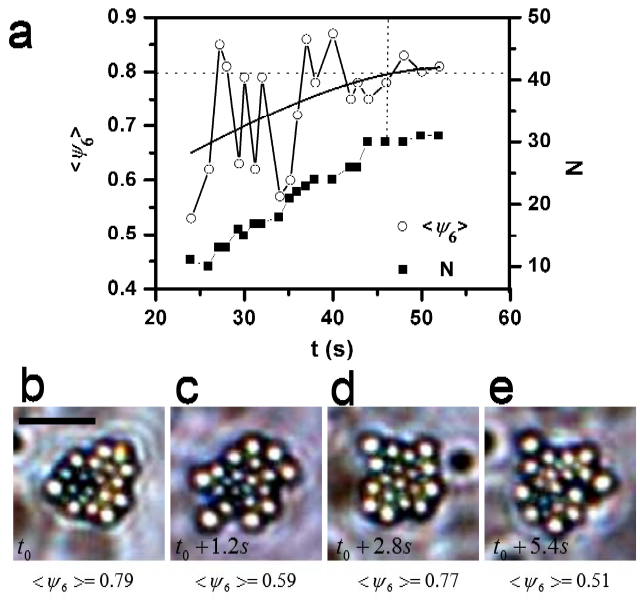

Figure 3.3 Precritical nuclei at high supersaturations exhibit structure fluctuations. (a): Fluctuation of order parameter during the growth. (b), (d): Due to the fluctuation, nuclei can have a transient crystalline structure. (c), (e): Liquid-like structure displayed by precritical nuclei. Scale bar: 10 μm.

According to Equation (3-2), given the same particle interaction and nucleus size, the reduction of the energy barrier between the metastable liquid-like structure and the

stable crystal-like structure should be attributed to the increase of $\mu_L - \mu_C$. The increase of $\mu_L - \mu_C$ would, as indicated by Equation (3.3), lead to the decrease of the ratio of n_b^* / n_s^*, which means that the transition size N_{trans} would become smaller at low frequencies (high supersaturations).

3. 5 Dependence of Transition Size on Supersaturation

N_{trans} is measured to be ~30 at *f*=3000 Hz, which is much smaller than the value (~80) measured at *f*=5000 Hz. A smaller N_{trans} means that given the same size, nuclei may have a higher order degree at high supersaturations. This can be seen by comparing Figures 3.2 and 3.3(a): in Figure 3.2, nuclei with size 10~20 have an average minimum $<\psi_6>$ around 0.5, while in Figure 3.3(a), nuclei with the same size have an average minimum $<\psi_6>$ around 0.6. This may explain why with the same magnitude fluctuation of $<\psi_6>$, nuclei with size 10~20 can acquire a transient crystal-like structure at *f*=3000Hz while they cannot do so at *f*=5000 Hz.

One should expect that at some high supersaturations, the transition size N_{trans} will become so small that crystal nuclei may nucleate with an ordered structure at the beginning. This is what we observed at *f*=2000 Hz and V_{pp}=2.5 V. In Figure 3.4, the nuclei are created from the beginning with crystalline structure which is identical to the structure of the mature crystals. This picture is in consistent with CNT as regards the structure of the nuclei. The observation shown in Figure 3.4 suggests that CNT may be a mechanism proceeding at high supersaturations for which the nucleation

barrier for crystallization is very small or may even vanish.

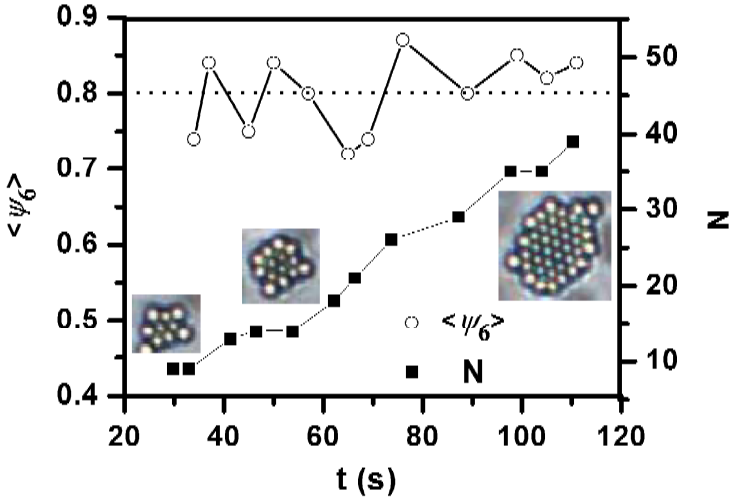

Figure 3.4 As supersaturation is high and thus the critical size is small enough, crystal nuclei are created with crystalline structure ($< \psi_6 > \sim 0.8$) as suggested by CNT.

3. 6 Conclusion

From the above observations, it is clear that at low or intermediate supersaturations, when the critical size is not small, a continuous structure transition will be adopted by the growing crystal nuclei due to surface effects. During the continuous structure transition, the exterior layer of the precritical nuclei is liquid-like. A direct consequence of the presence of a liquid surface layer is that surface tension is greatly reduced, and thus the nucleation energy barrier becomes substantially lower.

In summary, due to surface effects, we find that the structure of crystal nuclei will experience a continuous transition from the liquid-like to the crystal-like. This route ascribes to the nuclei a much lower free energy than either the entirely crystal-like or

liquid-like nuclei. This route will reduce the height of the nucleation energy barrier and thus enhance nucleation. This study suggests that critical nuclei are different from precritical nuclei not only in size but also in structure, as has been suggested recently by Moroni and ten Wolde et al.[5]

References

[1] J. J. De Yoreo and P. G. Vekilov, "Principles of Crystal Nucleation and Growth " *Rev Mineral Geochem*, vol. 54, pp. 57, 2003.

[2] V. M. Fokin, N. S. Yuritsyn, and E. D. Zanotto, "Nucleation and Crystallization Kinetics in Silicate Glasses: Theory and Experiment," in *Nucleation Theory and Applications*, J. W. P. Schmelzer, Ed.: Wiley-VCH Verlag GmbH & Co. KGaA 2005, pp. 74.

[3] A. Lomakin, N. Asherie, and G. B. Benedek, "Liquid-Solid Transition in Nuclei of Protein Crystals," *Proc. Natl. Acad. Sci. USA*, vol. 100, pp. 10254, 2003.

[4] J. P. K. Doye and F. Calvo, "Entropic Effects on the Size Dependence of Cluster Structure," *Phys. Rev. Lett.*, vol. 86, pp. 3570, 2001.

[5] D. Moroni, P. R. ten Wolde, and P. G. Bolhuis, "Interplay between Structure and Size in a Critical Crystal Nucleus," *Phys. Rev. Lett.*, vol. 94, pp. 235703, 2005.

[6] J. Anwar and P. K. Boateng, "Computer Simulation of Crystallization from Solution," *J. Am. Chem. Soc.*, vol. 120, pp. 9600, 1998.

[7] D. Kashchiev, *Nucleation: Basic Theory with Applications*: Butterworth-Heinemann, Oxford, 2000.

[8] A. Laaksonen, V. Talanquer, and D. W. Oxtoby, "Nucleation: Measurements, Theory, and Atmospheric Applications," *Annu. Rev. Phys. Chem.*, vol. 46, pp. 489, 1995.

Chapter 4 Multi-Step Crystallization

4. 1 Introduction

To explore robust experimental strategies for the control of crystallization, much attention has been focused on understanding the underlying mechanisms crystallization [1-3]. Among them, the route by which crystal nuclei approach their final stable crystalline structure is of fundamental importance. Our observations in Chapter 3 show that crystal nuclei would rather adopt a liquid-like structure at their earliest stage. In subsequent growth, the order degree of the crystal nuclei increases gradually with the size. In this process, the occurrence of the liquid-like structure is induced by surface effects.

However, it is possible in crystallization that a metastable liquid phase would first nucleate and subsequently a crystalline phase nucleate from the metastable liquid phase. According to Ostwald's rule [4], the phase occurring first in crystallization should be the one which is closest in free energy to the mother phase, that is, the least

stable phase, followed by phases in order of increasing stability. An intriguing example of Ostwald's rule is the so-called two-step crystallization (TSC) which has attracted much attention in the past decades.

TSC was originally suggested by ten Wolde and Frenkel [5]. They found by simulations that near the critical point of a liquid-liquid phase separation (LLPS), proteins crystallize through a two-step process: at the first step, amorphous dense droplets nucleate from the mother phase through LLPS; subsequently, crystalline nuclei nucleate from the amorphous dense droplets. Due to its significant implications in science and technology, TSC has been studied extensively in both theory [6-9] and experiment [10, 11] in protein solutions. However, recent studies suggested that this mechanism occurs not only in protein solutions, but also in typical atomic systems [12-14]. Lutsko et al. argued that TSC may be a mechanism underlying most crystallization processes in atomic systems [14]. Experimentally, this mechanism has been observed during the growth of nanocrystals [13]. Moreover, it has been found that TSC occurs also widely in bio-related crystallization [15]. For example, during the formation of calcite in sea urchin larvae, a transient amorphous phase is first formed, before the final crystal phase is reached [16, 17]. Similarly, a transient amorphous phase is identified in the formation of aragonite controlled by mollusk bivalve larvae [17, 18]. It is now widely believed that the development of crystalline structures with a well-defined shape and size in biological systems is essentially facilitated by the occurrence of transient amorphous phases [16, 17, 19].

A remarkable drawback of previous studies concerning TSC is that no direct investigation of the kinetic processes of TSC has been conducted. Therefore, in which way the occurrence of a transient amorphous precursor will affect and modify the formation of crystalline structures has so far not been addressed. A comprehensive understanding of this issue will advance our knowledge on multi-step crystallization, and provide a guideline in identifying robust experimental strategies for the engineering of crystalline structures. Despite its importance, however, the kinetics of stepwise crystallization such as TSC has so far remained unclear.

In this Chapter, the kinetics of crystallization via an amorphous precursor was studied using a colloidal model system. Our results were obtained from in situ observations at the single-particle level. The major purpose of this study is to address the kinetics of the creation of crystalline nuclei and their subsequent growth in an amorphous precursor. Furthermore, the kinetic advantages of crystallization via an amorphous precursor in producing high quality crystals were addressed. This information will provide an in depth understanding of the effect of amorphous precursors on crystal growth.

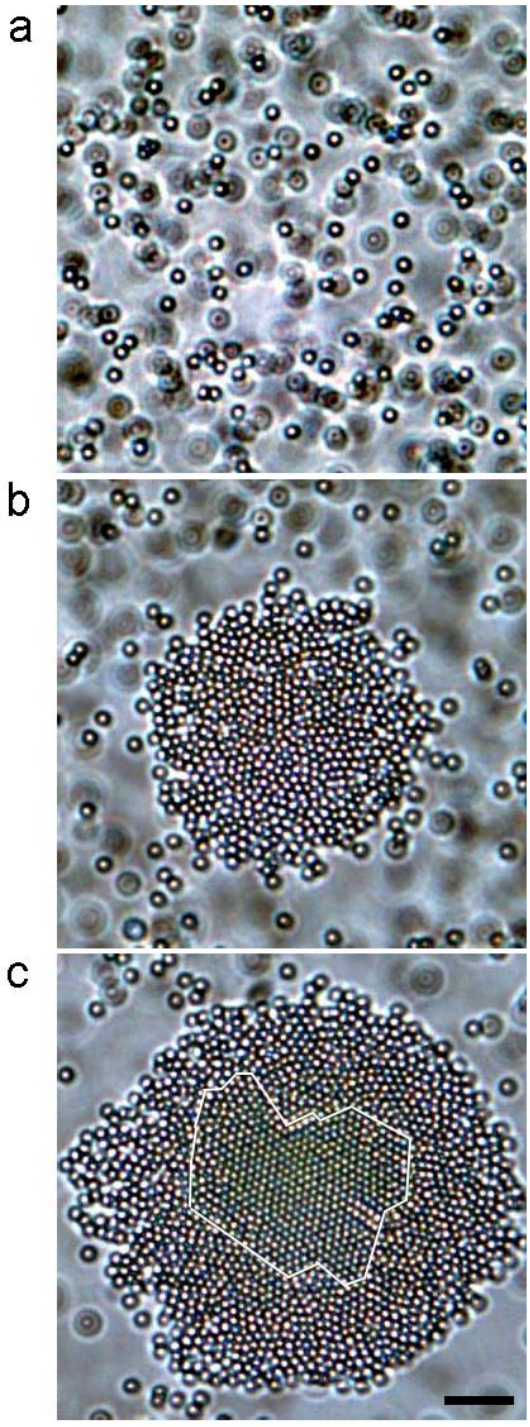

Figure 4.1 Multi-step crystallization observed at 800 Hz and 167 V/cm: (a) Initial dilute liquid phase. (b) Amorphous dense droplets are first created from the mother phase. (c) Crystalline nuclei are created from the amorphous phase. Scale bar: 10 μ m.

4. 2 Colloidal Suspension

In this study, the volume fraction of the colloidal suspension is 0.03%. The surface potential of the colloidal particles was adjusted to -72 mV by adding Na_2SO_4 with concentration 10^{-4} M. The pH of the suspension was measured to be 6.35. The phase diagram of this suspension was shown in Figure 2.2 (Chapter 2).

4. 3 Crystallization Mediated by an Amorphous Precursor

In our experiments, the most interesting phenomenon observed in the 2DC region (see Figure 2.2) is crystallization via an amorphous dense phase. A typical process is shown in Figure 4.1.

In our system, the mother phase is a dilute solution as shown in Figure 4.1(a). As the system is supersaturated by applying an AEF (f=800 Hz, **E**=167 V/cm), two-dimensional amorphous dense droplets are first formed on the glass surfaces as shown in Figure 4.1(b). Two-dimensional crystals are subsequently formed from the droplets as shown in Figure 4.1(c). Consistently with previous theoretical studies of TSC [6-9], the crystals are covered by a liquid film (Figure 4.1(c)). In this process, as suggested by Ostwald's rule, the amorphous dense droplets are first nucleated because their lower interfacial free energy (the 1D analog of the surface free energy), results in a lower nucleation energy barrier as compared with the crystals. Nevertheless, the subsequent nucleation of the crystalline phase in the droplets indicates that the amorphous phase is metastable with respect to the crystalline phase.

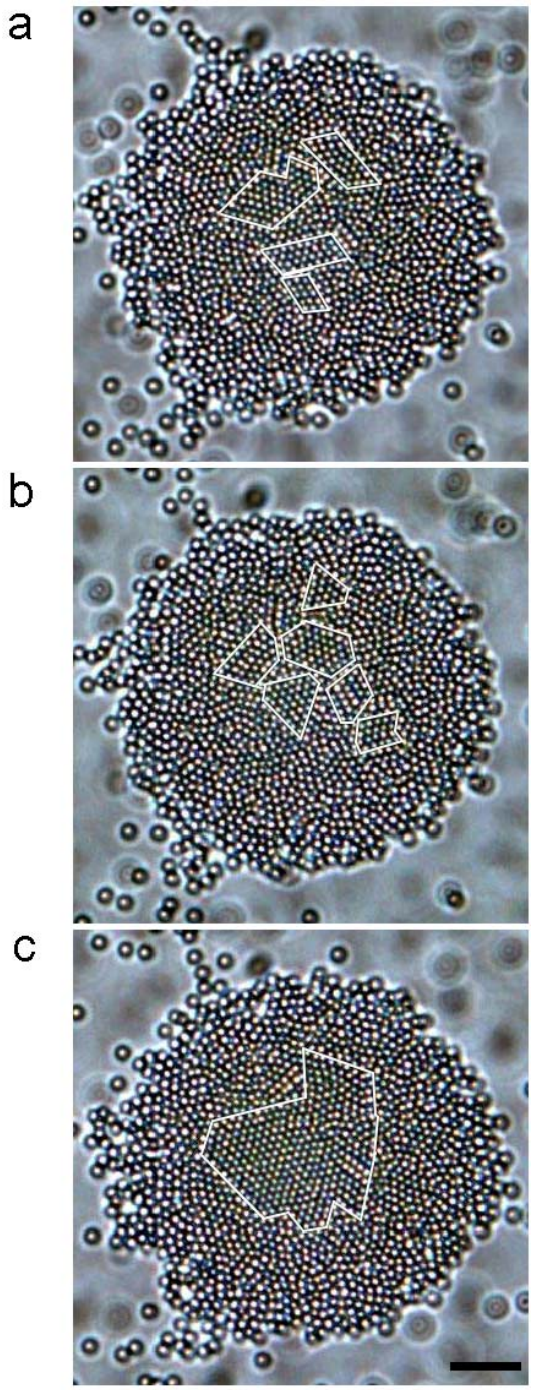

Figure 4.2 The evolution of the crystalline phase inside the amorphous phase: (a) Small sub-crystalline nuclei are initially created in the droplets. (b) More sub-crystalline nuclei are created as the droplet grows. (c) Stable mature crystalline nuclei are created from the dense droplets. Scale bar: 10 μm

The way of creating the initial crystalline nuclei from the metastable amorphous phases has never been addressed [6-14] due to the difficulty of directly observing the nucleation process in real space. In contrast to previous studies [6-14], in our system, the motion of individual colloidal particles can be traced in real-time and real-space, allowing us to follow the dynamic processes of the creation of the crystalline nuclei at the single-particle level. Taking advantage of this, the dynamics for the dense droplets in the course of creating crystalline nuclei was investigated in detail. A typical process is exhibited in Figure 4.2.

From Figure 4.2(a), it is found that initially, a few crystalline nuclei are created simultaneously from the dense droplets. Nevertheless, these small nuclei are unstable, namely, they are sub-crystalline nuclei. A detailed investigation shows that the sub-crystalline nuclei tend to shrink or dissolve soon after their creation, and subsequently, other sub-crystalline nuclei are formed randomly again. It is evident that the creation as well as the dissociation of the sub-crystalline nuclei in the dense droplets is governed by thermal fluctuations. As the number of sub-crystalline nuclei increases with the growth of the dense droplets, a stable mature crystalline nucleus will be finally created (Figure 4.2(c)). However, it is interesting to note that although a few sub-crystalline nuclei are created simultaneously at an early stage as shown in Figure 4.2(a), only one stable mature crystalline nucleus is possible in a dense droplet.

The fact that the formation of crystalline nuclei in the tiny droplets is subjected to thermal fluctuations, and several sub-crystalline nuclei will be created simultaneously,

was not realized in previous studies of TSC [6-11]. On the contrary, although not clearly stated, it was assumed [6-11] that a crystalline nucleus is formed and thus grows continuously from the beginning. Based on this assumption, the so-called mononuclear mechanism was developed [20]. It follows that once a crystalline nucleus is created from the dense droplets, it grows so fast that the formation of the second crystalline nucleus is suppressed. Based on the mononuclear mechanism, the overall nucleation rate of crystals in TSC was established. However, our observation shows that this assumption is not applicable in real experiments.

4. 4 Critical Sizes of MSC

The process shown in Figure 4.2 suggests that crystalline nuclei are not stable Form this process, it is found that in the dense droplets, crystalline nuclei have to get large enough in order to become stable.

To quantify the crystallization process and identify the critical size for the crystalline nuclei, the local two-dimensional bond-order parameter $\psi_6(r_i)$ as introduced in Chapter 2 is employed to identify the crystal-like particles inside the amorphous colloidal clusters.

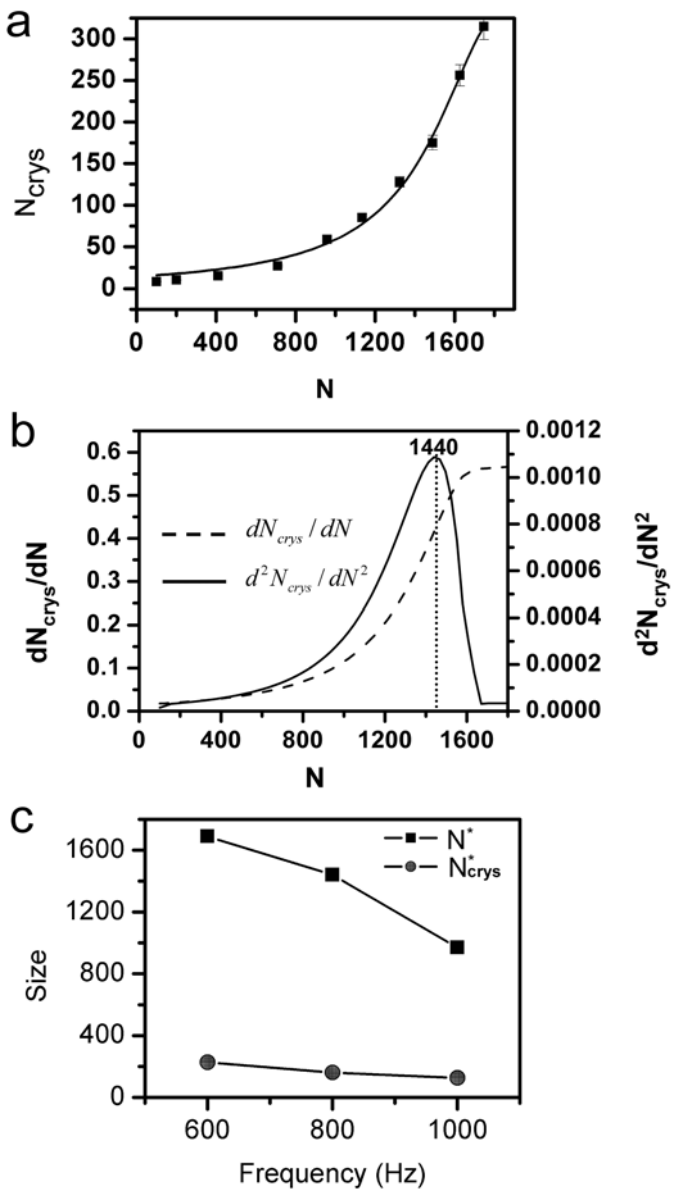

Figure 4.3 The critical sizes of MSC: (a) Dependence of N_{crys} on N in a typical MSC (f=800 Hz and E=167 V/cm). (b)The critical size of crystalline nuclei N^*_{crys} is identified from the maximum of d^2N_{crys}/dN^2. (c) Dependence of N^*_{crts} and N^* on frequency under condition of E =167 V/cm.

Using ψ_6, the crystallization process as illustrated by Figures 4.1 and 4.2 was analyzed quantitatively. The dependence of the number of crystal-like particles N_{crys} on the size of the dense droplets N is plotted in Figure 4.3(a). The N_{crys} vs N plot consists of three regimes in terms of N. Regime I (linear regime): $N < 1000$.

The increase of N_{crys} is essentially proportional to the increase of N, giving rise to a small slope dN_{crys}/dN ~0.03. Regime II (nonlinear regime): 1000< N <1400. The plot N_{crys} vs N is a curve, dN_{crys}/dN rising continuously with N. Regime III (linear regime): N >1400. dN_{crys}/dN remains constant and N_{crys} becomes linearly dependent on N again, giving rise to a relatively much larger $dN_{crys}/dN \sim 0.45$. Further investigation reveals that as N increases beyond 1400, the crystalline structure in the dense droplets is represented by a mature crystalline nucleus as shown in Figure 4.2(c). It is clear that the fast steady increase of N_{crys} as N >1400 is due to the existence of the mature crystalline nucleus, which acts as a stable core for subsequent crystal growth, while the slow steady growth of N_{crys} when N is less than 1000 should be attributed to the co-occurrence of dissociation and creation of crystalline nuclei. Accordingly, the creation of a critical crystalline nucleus should be responsible for the termination of the continuous rise of dN_{crys}/dN in Regime II. Based on the above reasoning, d^2N_{crys}/dN^2 should approach its maximum when the amorphous dense droplets reach a critical size N^* and thus are able to form a crystalline critical nucleus with size N^*_{crys}. d^2N_{crys}/dN^2 was derived as a function of N by differentiating the fit of the dependence of N_{crys} on N. As shown in Figure 4a, d^2N_{crys}/dN^2 approaches its maximum at $N^* \sim 1440$. The corresponding N^*_{crys} is measured to be ~161. Here, it is clear that to accommodate a critical crystalline nucleus, an amorphous dense droplet needs to first acquire a critical size N^*. Compared with previous results of TSC [6-14], the stepwise crystallization in our

experiments is characterized by the fluctuation-governed dynamics of creating crystalline nuclei and the critical sizes N^*_{crys} and N^*. To notice this difference, multi-step crystallization (MSC) is used to establish the special crystallization processes observed in our experiments.

In our experiments, both critical sizes N^*_{crys} and N^* in MSC are a function of supersaturation which in our system is dependent on both frequency f and the strength of the electric field E [21]. Figure 4.3(b) shows that increasing frequency leads to a decrease of both of N^*_{crys} and N^*. However, compared with the decrease of N^*, the change of N^*_{crys} is minor, indicating that at high frequencies, the dense droplets are likely to create a mature crystalline nucleus at an earlier stage in terms of N. This indicates that the relative supersaturation in the dense droplets for the nucleation of the crystalline phase might be enhanced by increasing the frequency.

We have discussed above that the sub-crystalline nuclei in the metastable amorphous droplets are created by thermal fluctuations. However, it is surprising to find that the stable mature crystalline nuclei are not created by thermal fluctuations, but by the coalescence of the sub-crystalline nuclei. As the time sequence in Figure 4.2 shows, accompanying the sharp increase of dN_{crys}/dN in the region of $1000 < N < 1400$, the average number of sub-crystalline nuclei increases as can be seen from Figures 4.2(a) and Figure 4.2(b). As a consequence, the sub-crystalline nuclei approach one another in the dense droplets. Finally, these sub nuclei meet and coalesce. However, at the early stage, the result of the coalescence is usually a

crystalline nucleus smaller than N^*_{crys}, which normally breaks up again into sub-crystalline nuclei. Once a crystalline nucleus larger than N^*_{crys} is coalesced, it will remain stable, functioning as a growth center for subsequent growth.

Because our system is a limit system, it is not an ideal homogeneous system. Quantitative results, such as N^*_{crys} and N^*, may be different at different regions. Therefore, the measurements are usually carried out at the same region under different frequency and electric filed strength. Normally, there is only one amorphous droplet within the observation window can reach the critical size N^* and experience a successful MSC. Normally observations will be repeated two or three time at the same region. It was found at the same region and same conditions, results of measurement are essentially the same. Although the quantitative results may change at different observation regions, the general mechanism of MSC discussed above is the same.

4. 5 Elimination of Grain Boundaries

The final mature crystals in the dense droplets are, to a large extent, free from defects, such as grain boundaries, as can be seen in Figures 4.1(c) and 4.2(c). However, since the sub-crystalline nuclei as shown in Figures 4.2(a) and 4.2(b) usually do not match one another's orientations before they coalesce, grain boundaries are expected to appear in the final crystals. In fact, grain boundaries actually exist in the initial mature crystals, but they are eliminated gradually during

the following growth. The kinetics of the defect elimination is illustrated by the time sequence shown in Figure 4.4.

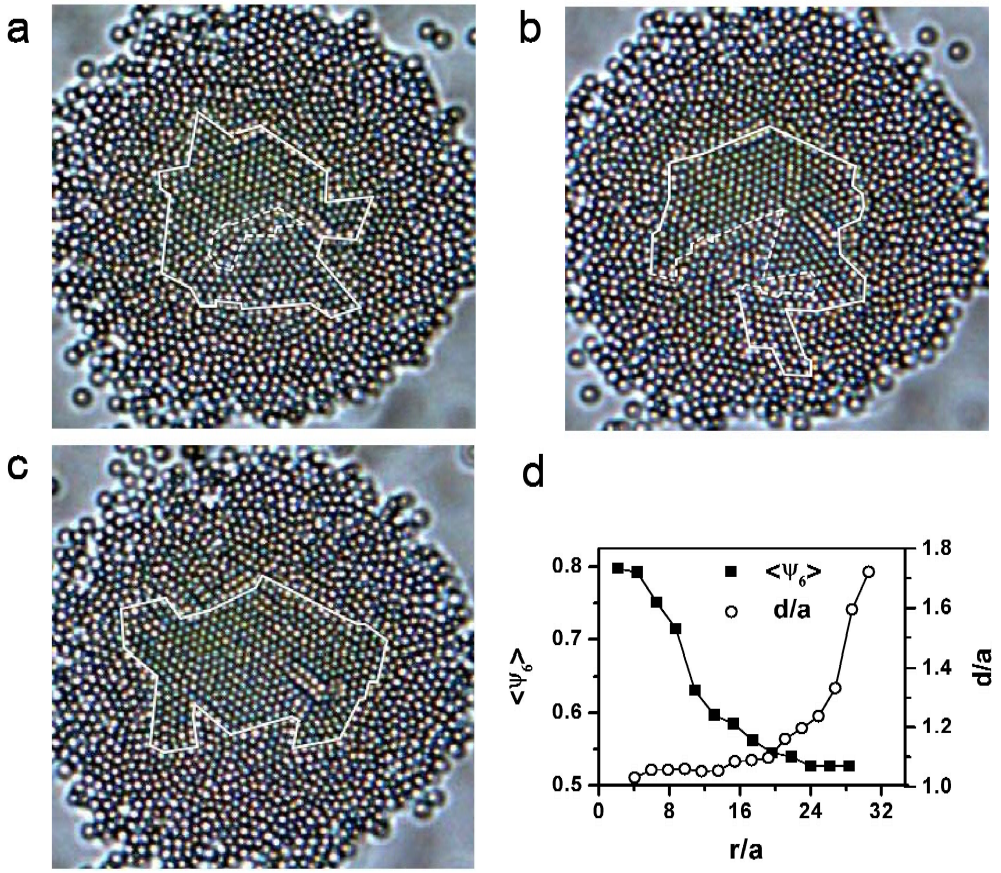

Figure 4.4 Elimination of grain boundaries: (a) Grain boundaries (encircled by a dashed line) are created during the coalescence. (b) A local transformation from crystalline phase to amorphous phase is adopted to release the strain. (c) Quality of the crystalline structure is highly improved after the elimination. (d) The order degree in terms of $< \psi_6 >$ and the average center-to-center distance d as a function of the distance r to the mass center of the colloidal cluster shown in Figure 4.4(c). The gradual increase of d is a direct reflection of the gradual decrease of density. a is the diameter of the colloidal particles.

Initially, a grain boundary exists in the mature crystal as shown in Figure 4.4(a). However, in the following process, part of the crystalline structure adjacent to the grain boundary melts and becomes amorphous as shown in Figure 4.4(b). We

suggest that this local transition from the crystalline phase to the amorphous phase is triggered by the strain contained in the grain boundary. By this local crystal-liquid transition, the strain is released, and most importantly, the particles involved get a chance to rearrange themselves along the orientations defined by the remaining crystalline structure. As a result, the orientations are unified considerably (Figure 4.4(c)). Normally, the removal of grain boundaries needs to break the surface bonds of the crystals due to the interfacial tension, and thus energy is needed to initiate this process. Nevertheless, during the process shown in Figure 4.4, no additional energy is input. It seems that the local crystal-liquid transition shown in Figure 4.4 is free of an energy barrier.

An important feature of the colloidal clusters as shown in Figures 4.4(a)-(c) is that both the order degree and density in the dense droplets decrease continuously from the crystalline core to the amorphous fringe. A quantitative description of the continuous change in the cluster shown in Figure 4.4(c) is presented in Figure 4.4(d). The 'free' local crystal-liquid transition can be well understood after taking note of this continuous change in the order degree and the density. Interfacial tension is normally induced by a sharp change in density or in structure on the interface. However, in our experiments, due to the continuous change in the density and the order degree, there is an intermediate region in the dense droplets between the crystalline core and the amorphous fringe. In the intermediate region, the density in the interior adjacent to the crystalline core is almost identical to the crystalline phase,

and the arrangement of colloidal spheres there is also ordered or at least partially ordered. In fact, it is hard to define an interface between the crystalline phase and the amorphous phase in the dense droplets due to the existence of the intermediate region. The particles in this region are just as likely to become crystal-like as well as liquid-like by fluctuations. Therefore, the intermediate region is able to allow a crystal-liquid transition, whereby the grain boundaries are eliminated. Moreover, through the transition from crystal to liquid, crystal-like particles incorrectly incorporated in the intermediate region can easily become liquid-like again and get one more chance to incorporate themselves. This advantage can significantly inhibit the creation of defects caused by incorrect incorporations.

4.6 Overall Nucleation Rate of Crystals in MSC

Another advantage of MSC proposed by previous studies of TSC [6-11] is that the nucleation of amorphous dense droplets occurs much faster than the nucleation of a crystalline phase due to its lower free energy barrier. And subsequently, the larger density in the dense droplets will in turn enhance the nucleation of the crystalline phase. Consequently, the overall nucleation of the crystalline phase will be enhanced. To quantify the enhancement of the nucleation of crystals, the overall nucleation rate J_c of crystals in TSC was calculated by Kashchiev et al [20] on the so-called mononuclear assumption. It was found that the overall nucleation rate J_c of the crystal at a stationary stage was equal to the nucleation rate J of the dense droplet.

Since J is much larger than for crystals nucleated directly from the mother phase, it follows that the overall nucleation rate of the crystal is actually enhanced. However, the mononuclear mechanism does not hold in real experiments as we discussed above. Another important assumption contained in the conclusion of Kashchiev et al. was that every dense droplet is able to develop a mature crystalline nucleus. However, contrary to this assumption, it was found that although a good deal of dense droplets were created at an early stage, most of them disappeared gradually, and only a few succeeded in developing into a stable crystal [11]. Similarly, in our system, due to the existence of a critical size N^* for dense droplets, under the conditions f =800 Hz and E =167 V/cm, normally only three or four out of twenty dense droplets can grow beyond the critical size N^* and thus create a stable crystalline nucleus. Other droplets disappear gradually and their matter is transported to the droplets containing a stable crystal. Therefore, the conclusion in previous studies [6-11] that the presence of an amorphous precursor can enhance the overall nucleation of the crystal becomes questionable. It is possible that, although only a part of the dense droplets can allow the nucleation of a crystal, the effective overall nucleation rate of the crystal is still much higher than that of the crystals nucleated directly from the mother phase. However, it is also possible that the nucleation of the crystal in the dense droplets is not fast enough to support an enhancement of the overall nucleation rate of the crystal. Therefore, whether or not the overall nucleation rate of the crystal in MSC is enhanced will, to a large extent, be determined by the crystal nucleation processes in

the dense droplets, as well as the nucleation rate of the dense droplets. However, since every droplet can produce only one mature crystalline nucleus, the conventional method of measuring nucleation rates by counting the number of nuclei as a function of time is no longer applicable. Thus, a special method has to be developed, and it will be addressed in Chapter 5.

4. 7 Mechanism Underlying MSC

TSC or MSC in protein solutions has been believed to be induced by short-range attractions [6-11]. However, experimentally, TSC or MSC had previously not been observed in colloids where only short-range attractions operate. In practice, when TSC was expected to take place, colloids with only short-range attractions were usually confined in gel-like states [22-24]. Noro et al. found that an additional long-range attraction can shift the critical point of LLPS of colloids with short-range attractions out of the gel region [24]. Consequently, they argued that long-range attractions may be important for the mechanism of TSC, and the experimentally observed TSC in protein solutions [10, 11], as Noro et al. argued, should be attributed to some less-known long-range attractions. This argument is supported by a recent experimental study, in which it was found that a weak long-range attraction does indeed exist between protein molecules in solutions [25]. Moreover, the latest simulation carried out by Lutsko et al.[14] suggested that in typical atomic systems, where attractions are relatively long-range, TSC is favored and may underlie most of

the crystallization processes. All these studies suggested that the relation between TSC and short-range attractions may be incompletely understood, and that long-range attractions may play an important role in the mechanism of TSC.

In our system, a long-range attraction exists between colloidal particles. This long-range attraction is induced by an electrohydrodynamic (EHD) mechanism. Both the range and the strength of this long-range attraction are dependent on the frequency as well as on the strength of the electric field [26-29]. Experimentally, this long-range attraction has to be mediated by fluid flow. Therefore, it should no longer work inside the droplets or the crystals where fluid flow becomes negligible [30]. In this case, we suggest that a short-range attraction exists between colloidal particles, working to balance the electrostatic repulsion between colloidal particles inside the droplets. This short-range attraction may arise from an electrostatic ion-ion correlation [31]. According to the argument of Noro et al.[24], the short-range attraction in our system plays the role of inducing the metastable LLPS and maintaining the presence of the metastable dense droplets, while the long-range EHD attraction works to shift the LLPS from a possible gellation region.

4. 8 Two-Dimensional and Three-Dimensional MSC

An important characteristic of this study is that the system under investigation is two-dimensional. In practice, two-dimensional (2D) nucleation is an important mechanism underlying aggregations occurring on interfaces [32, 33]. Moreover, for

dislocation-free crystals, the growth of faceted crystal faces is governed by a 2D nucleation mechanism [34, 35]. Similarly to 3D nucleation, both homogeneous and heterogeneous nucleation can occur in 2D systems [34, 36]. The studies of 2D homogeneous and heterogeneous nucleation have revealed that the mechanisms underlying 2D nucleation are essentially similar to 3D nucleation [21, 36, 37]. In other words, the general conclusions obtained in 2D nucleation are normally readily applicable to 3D nucleation. In this study, MSC is examined in a two-dimensional system. However, three-dimensional MSC has already been observed in simulations and experiments [17, 18]. Comparing our results with previous studies, it is found that the mechanisms of the 2D MSC observed in our experiments are consistent with previous studies of 3D MSC in several characteristics: First, a metastable liquid-like precursor is first nucleated; Second, crystalline nuclei are subsequently created from the metastable precursor; Finally, the density decreases gradually from the crystalline core to the liquid-like fringe. Based on the above knowledge, it is reasonable to conclude that the key results of this study about MSC, including the mechanism of creating sub-crystalline nuclei from the metastable liquid-like precursor, the kinetics underlying the formation of the critical crystalline nuclei, the continuous change of concentration and structure in the metastable liquid clusters and its advantages in eliminating defects are readily applicable to a 3D MSC.

4. 9 Conclusions

In this study, two-dimensional crystallization via a metastable amorphous phase was studied in a colloidal model system. It is found that the crystalline nuclei in the metastable dense droplets are initially created by fluctuation, and it is necessary for them to acquire a critical size before they can remain stable and grow steadily. Every droplet can produce only one mature crystalline nucleus. In contrast to the creation of sub-crystalline nuclei, the mature crystalline nuclei may be created by the coalescence of sub-crystalline nuclei. Initially, a mature crystalline nucleus is created with grain boundaries. To eliminate the grain boundaries, a local structure transition from crystal to liquid is adopted to release the strain contained by grain boundaries. This kind of transition is supported by the continuous change of the density and the structure in the dense droplets.

It is reasonable to suggest that the kinetics observed in this study may also govern protein crystallization because globular proteins can be well modeled by colloidal hard spheres. Furthermore, our observations of MSC may serve as an illustration of how biomineralization may proceed with the presence of an amorphous metastable phase. We believe that the results presented in this article may offer a basis for further critical study.

References

[1] S. Piana and J. D. Gale, "Understanding the Barriers to Crystal Growth: Dynamical Simulation of the Dissolution and Growth of Urea from Aqueous Solution," *J. Am. Chem. Soc.*, vol. 127, pp. 1975, 2005.

[2] S. Piana, F. Jones, and J. D. Gale, "Assisted Desolvation as a Key Kinetic Step for Crystal Growth," *J. Am. Chem. Soc.*, vol. 128, pp. 13568, 2006.

[3] J. Anwar and P. K. Boateng, "Computer Simulation of Crystallization from Solution," *J. Am. Chem. Soc.*, vol. 120, pp. 9600, 1998.

[4] W. Ostwald, "Studien über die Bildung und Umwandlung fester Körper," *Z. Phys. Chem.* , vol. 22, pp. 289, 1897.

[5] P. R. ten Wolde and D. Frenkel, "Enhancement of Protein Crystal Nucleation by Critical Density Fluctuations," *Science*, vol. 277, pp. 1975-1978, 1997.

[6] V. Talanquer and D. W. Oxtoby, "Crystal nucleation in the presence of a metastable critical point," *J. Chem. Phys.* , vol. 109, pp. 223 1998.

[7] C. Haas and J. Drenth, "Understanding protein crystallization on the basis of the phase diagram," *J. Cryst. Growth* vol. 196, pp. 388 1999.

[8] C. Haas and J. Drenth, "The Interface between a Protein Crystal and an Aqueous Solution and Its Effects on Nucleation and Crystal Growth " *J. Phys. Chem. B* vol. 104, pp. 368, 2000.

[9] A. Shiryayev and J. D. Gunton, "Crystal nucleation for a model of globular proteins," *J. Chem. Phys.*, vol. 120, pp. 8318, 2004.

[10] Y. G. Kuznetsov, A. J. Malkin, and A. McPherson, "The liquid protein phase in crystallization: a case study-intact immunoglobulins," *J. Cryst. Growth*, vol. 232 pp. 30-39, 2001.

[11] P. G. Vekilov, "Dense Liquid Precursor for the Nucleation of Ordered Solid Phases from Solution," *Crys. Growth & Design*, vol. 4, pp. 671-685, 2004.

[12] P. R. ten Wolde and D. Frenkel, "Homogeneous nucleation and the Ostwald step rule," *Phys. Chem. Chem. Phys.*, vol. 1, pp. 2191, 1999.

[13] X. Chen, A. C. S. Samia, Y. Lou, and C. Burda, "Investigation of the Crystallization Process in 2 nm CdSe Quantum Dots," *J. Am. Chem. Soc.*, vol. 127, pp. 4372-4375, 2005.

[14] J. F. Lutsko and G. Nicolis, "Theoretical Evidence for a Dense Fluid Precursor to Crystallization," *Phys. Rev. Lett.*, vol. 96, pp. 046102, 2006.

[15] L. Addadi and S. Weiner, "Control and Design Principles in Biological Mineralization," *Angew. Chem. Int. Ed. Engl.* , vol. 31, pp. 153 1992.

[16] E. Beniash, J. Aizenberg, L. Addadi, and S. Weiner, "Amorphous calcium carbonate transforms into calcite during sea urchin larval spicule growth," *Proc. R. Soc. London Ser. B*, vol. 264, pp. 461, 1997.

[17] L. Addadi, S. Raz, and S. Weiner, "Taking Advantage of Disorder: Amorphous Calcium Carbonate and Its Roles in Biomineralization," *Adv. Mater.* , vol. 15, pp. 959, 2003.

[18] I. M. Weiss, N. Tuross, L. Addadi, and S. Weiner, "Mollusc larval shell formation: amorphous calcium carbonate is a precursor phase for aragonite," *J. Exp. Zool.*, vol. 293, pp. 478, 2002.

[19] I. M. Wiss, N. Tuross, L. Addadi, and S. Winer, *J. Exp. Zool.*, vol. 293, pp. 478, 2002.

[20] D. Kashchiev, P. G. Vekilov, and A. B. Kolomeisky, "Kinetics of two-step nucleation of crystals," *J. Chem. Phys.*, vol. 122, pp. 244706, 2005.

[21] K.-Q. Zhang and X. Y. Liu, "In situ observation of colloidal monolayer nucleation driven by an alternating electric field," *Nature*, vol. 429, pp. 739, 2004.

[22] K. G. Soga, J. R. Melrose, and R. C. Ball, "Metastable states and the kinetics of colloid phase separation," *J. Chem. Phys.*, vol. 110, pp. 2280, 1999.

[23] V. J. Anderson and H. N. W. Lekkerkerker, "Insights into phase transition kinetics from colloid science," *Nature*, vol. 416, pp. 811, 2002.

[24] M. G. Noro, N. Kern, and D. Frenkel, "The role of long-range forces in the phase behavior of colloids and proteins," *Europhys. Lett.*, vol. 48 pp. 332-338, 1999.

[25] Y. Liu, E. Fratini, P. Baglioni, W.-R. Chen, and S.-H. Chen, "Effective Long-Range Attraction between Protein Molecules in Solutions Studied by Small Angle Neutron Scattering," *Phys. Rev. Lett.*, vol. 95, pp. 118102, 2005.

[26] S.-R. Yeh, M. Seul, and B. I. Shraiman, "Assembly of ordered colloidal aggregrates by electric-field-induced fluid flow," *Nature* vol. 386, pp. 57, 1997.

[27] M. Trau, D. A. Saville, and I. A. Aksay, "Assembly of colloidal crystals at electrode interfaces," *Langmuir*, vol. 13, pp. 6375, 1997.

[28] P. J. Sides, "Calculation of Electrohydrodynamic Flow around a Single Particle on an Electrode," *Langmuir*, vol. 19, pp. 2745, 2003.

[29] F. Nadal, F. Argoul, P. Hanusse, B. Pouligny, and A. Ajdari, "Electrically induced interactions between colloidal particles in the vicinity of a conducting plane," *Phys. Rev. E*, vol. 65, pp. 061409, 2002.

[30] J. Santana-Solano, D. T. Wu, and D. W. M. Marr, "Direct Measurement of Colloidal Particle Rotation and Field Dependence in Alternating Current Electrohydrodynamic Flows," *Langmuir*, vol. 22, pp. 5932, 2006.

[31] J. P. Hansen and H. Löwen, *Annu. Rev. Phys. Chem.* , vol. 51, pp. 209, 2000.

[32] X. C. Zeng, "Gas-liquid nucleation in two-dimensional fluids," *J. Chem. Phys. 104*, vol. 104, pp. 2699, 1996.

[33] R. P. Richter, J. L. K. Him, B. Tessier, C. Tessier, and A. R. Brisson, "On the Kinetics of Adsorption and Two-Dimensional Self-Assembly of Annexin A5 on Supported Lipid Bilayers," *Biophys. J.*, vol. 89, pp. 3372, 2005.

[34] X. Y. Liu, K. Maiwa, and K. Tsukamoto, "Two-dimensional heterogeneous nucleation and the growth kinetics," *J. Chem. Phys.* , vol. 106, pp. 1870, 1997.

[35] D. Kashchiev, "Two-dimensional nucleation in crystal growth: thermodynamically consistent description of the nucleation work," *J. Cryst. Growth*, vol. 267, pp. 685, 2004.

[36] X. Y. Liu, "New understading for two-dimensional nucleation (II)," *Surf. Rev. Lett.*, vol. 8, pp. 423, 2001.

[37] X. Y. Liu, "New understading for three-dimensional nucleation (I)," *Surf. Rev. Lett.*, vol. 8, pp. 415, 2001.

Chapter 5 Nucleation Rate of Multi-Step Crystallization

5.1 Introduction

An important issue in the study of MSC is the estimate of the overall nucleation rate of crystals. As we have discussed in 4.6, a number of previous studies suggested that the occurrence of the metastable amorphous dense droplets may greatly enhance the nucleation of the crystalline phase [1-5]. A basic assumption underlying these studies is that all dense droplets can grow large enough to develop a crystal. However, a good deal of experimental evidence shows that although many dense droplets were created initially, only a fraction of them could successfully produce a crystal [6, 7]. In our experiments, only three or four out of twenty dense droplets can grow big enough to create a stable crystalline nucleus. Consequently, whether the occurrence of the metastable dense droplets can enhance the overall nucleation rate of the crystals

becomes questionable in practice. In the case of MSC observed in our experiments, it is found that to identify the overall nucleation rate J_c of the crystals, the estimate of the local nucleation rate of the crystalline phase in the droplets, which is hereafter denoted by j_c, is crucial. Nevertheless in previous studies [6, 7] due to the difficulties in conducting an *in-situ* observation of the crystal nucleation proceeding in the metastable amorphous droplets, j_c has never been determined experimentally.

In this Chapter, based on our observation of MSC presented in Chapter 4, a mathematical method is developed to deal with the local nucleation rate j_c of the crystals in the amorphous precursor.

5. 3 Method of Determining Nucleation Rate of MSC

Conventionally, the nucleation rate J is defined by:

$$J(t) = \frac{n(t)}{tV} \tag{5-1}$$

where $n(t)$, that is a function of time t, is the number of critical nuclei created from the mother phase within a volume of *V*. At a stationary state, $n(t)$ increases linearly with time and the nucleation rate J is time-independent [8]. In practice, to determine the nucleation rate, the number of nuclei is counted as a function of time, and J is evaluated from the slope of the linear part of the n vs t plot. However, Equation (5-1) loses its capacity to determine the local nucleation rate j_c of MSC because in most cases a droplet can produce only one crystalline nucleus, and

therefore the conventional method by counting the number of crystalline nuclei as a function of time fails. It is clear that, a different approach has to be developed.

At the stationary state, Equation (5-1) can be simplified to a time-independent form [9]:

$$J = \frac{1}{\tau V} \tag{5-2}$$

where τ is the average period needed by a mother phase with volume V to nucleate a new nucleus of the new phase. We assume that in MSC, Equation (5-2) can be approximately applied to j_c. To calculate the two-dimensional j_c, Equation (5-2) needs to be rewritten as:

$$\frac{1}{j_c} = \tau_A \cdot A \tag{5-3}$$

where τ_A is the time needed for an amorphous droplet with area A to create a crystal nucleus with critical size N^*_{crys}. Given a constant supersaturation, j_c is independent of time and A. Therefore at a given supersaturation, droplets with different A share a common feature: $\frac{1}{j_c}$. However, in our experiments, A increases with time as the droplets grow. It follows that Equation (5-3) should be modified in the form of an integral over time before it can be applied to a growing subsystem. Equation (5-4) gives result of the modification.

$$\frac{1}{j_c} = \int_0^{\tau} dt \cdot A(t) \tag{5-4}$$

where τ is the time a growing droplet takes to reach the critical size N^* and form a critical crystal nucleus with size N^*_{crys}.

To evaluate the nucleation rate j_c from Equation (5-4), τ and *A(t)* have to be first established. In practice, $A(t)$ is related to the size $N(t)$ by: $A(t) = N(t) * \pi(\frac{d_0}{2})^2$. Here, $N(t)$ is the total number of particles contained in the growing droplets, d_0 is the average center-to-center distance between two neighbor liquid-like colloidal particles in the amorphous droplets, and $\pi(\frac{d_0}{2})^2$ gives the average area occupied by a liquid-like particles in the droplets. Consequently, j_c can be evaluated from $N(t)$ by:

$$\frac{1}{j_c} = \int_0^{\tau} dt\ A(t) = \pi(\frac{d_0}{2})^2 \cdot \int_0^{\tau} dt\ N(t) \qquad (5\text{-}5)$$

$N(t)$ can be established directly from the experimental investigations. Nevertheless, τ, the nucleation time lapse needed by the amorphous droplets to create a critical crystal nucleus cannot be identified directly from experiments.

5. 4 Results of Nucleation Rates of MSC

In order to determine the time τ, we must first determine the size N^*_{crys} of the critical crystal nuclei in the amorphous droplets. The meaning of N^*_{crys} and N^* and how to determine their values have been introduced in section 4.4. When N^*_{crys} and N^* are known, τ can be determined from the experimentally established $N(t)$. In section 4.4, N^*_{crys} and N^* under conditions *f*=800 Hz and *E* = 167 V/cm are measured as ~161 and ~1440, respectively. Then from the curve $N \sim t$ (Fig. 5.1), τ

is measured at ~275 *s*. At the same conditions, d_0 is measured to be $1.24 \pm 0.02\ \mu m$. With the experimentally established $N(t)$, the numerical integration yields: $\int_0^{275} N(t)\,dt = 223399$. Substitution of the above results into Equation (5-5) gives $j_c \sim 3.7 \times 10^{-6}\ \mu m^{-2} s^{-1}$.

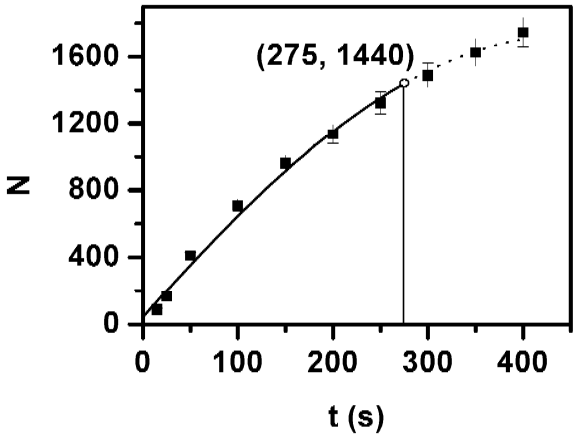

Figure 5.1 The plot of $N \sim t$ (f=800 Hz, E = 167 V/cm). The time when N reaches the critical size N^* is just the time τ needed by the growing droplets to create a critical crystal nucleus.

In our experiments as can be seen in Figure 5.2(a), j_c increases with frequency. This result, according to CNT, indicates that increasing frequency leads to an increase of the supersaturation for crystallization in the dense droplets. This is supported by the result shown in Figure 4.3(b). Figure 4.3(b) shows that the critical size N^*_{crys} decreases with frequency. This, according to Equation (1-2), means that the supersaturation is enhanced due to the increase of frequency. Moreover, as shown in Figure 5.2(b), d_0 decreases with frequency, that is, the particle density in the amorphous droplets becomes larger at high frequencies, which will directly enhance

the supersaturation for the local crystallization proceeding in the amorphous droplets.

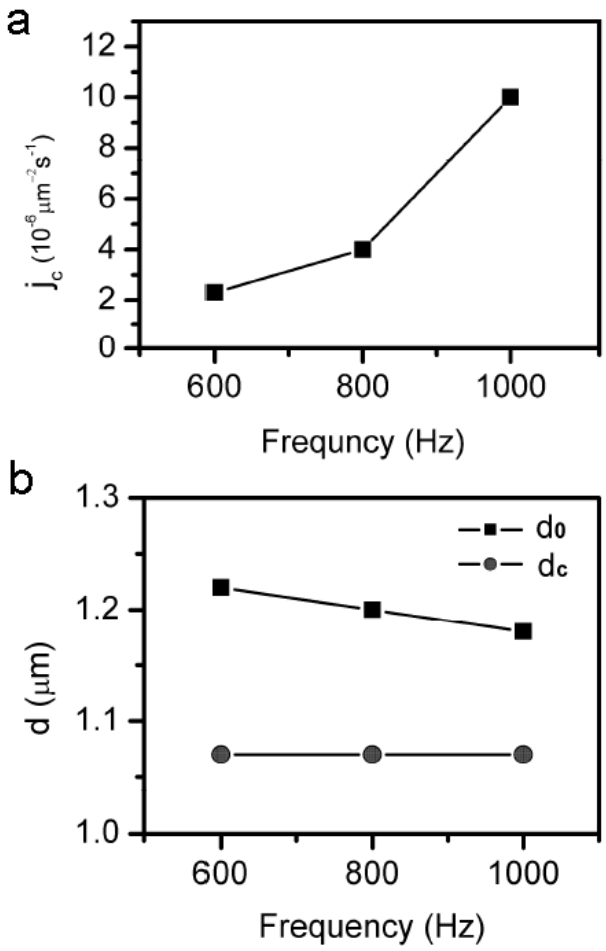

Figure 5.2 Dependence of MSC on frequency: (a) The local nucleation rate j_c increases with frequency. (b) The average distance d_0 in the liquid region between two neighbor 'liquid-like' particles decreases with frequency while the average distance d_c in the crystalline core between two neighbor 'crystal-like' particles remains essentially constant in the crystal core.

5. 5 Supersaturation and Interface Tension in the Amorphous Precursor

The information of the supersaturation is critical for the estimation of the nucleation barrier and the crystal-liquid interfacial free energy in the dense droplets.

According to CNT, the nucleation rate is related to the nucleation energy barrier ΔG^* by:

$$J = C\exp\left(-\frac{\Delta G^*}{k_B T}\right) \tag{5-6}$$

ΔG^* is determined by the thermodynamic driving force $\Delta\mu$ and the interfacial free energy γ [9]. In the case of two-dimensional nucleation, ΔG^* is given by:

$$\Delta G^* = \frac{\pi\gamma^2 s}{\Delta\mu} \tag{5-7}$$

where s is the average area occupied by the 'crystal-like' particle, which is determined by $s = \pi d_c^2/4$. d_c is the average center-to-center distance between two neighbor particles in the crystalline nuclei, which is experimentally measured to be $1.07 \pm 0.02\,\mu m$. Figure 5.2(b) shows that d_c essentially remains constant at different frequencies. The increase of j_c suggests that ΔG^* is reduced by increasing frequency. According to Equation (5-7), the reduction of ΔG^* can be caused by either the decrease of γ or the increase of the thermodynamic driving force $\Delta\mu$. In our case, $\Delta\mu$ can be defined in terms of the concentration c [8]:

$$\Delta\mu = k_B T \ln(c_0 / c_m) \tag{5-8}$$

where c_0 is the actual particle concentration of in the droplets and c_m is the equilibrium concentration of the droplets below which crystal nuclei cannot be created from the droplets. The particle concentration c in the droplets is connected to the average distance d_0 by $c = 4/\pi d_0^2$. Thus, Equation (5-8) can be rewritten as:

$$\Delta\mu = k_B T \ln(d_m^2 / d_0^2) \tag{5-9}$$

In our study, d_0 is measured experimentally and the result is shown in Figure 5.2(b). However it is difficult to determine d_m, the center-to-center distance corresponding to the equilibrium concentration c_m. But for determining $\Delta\mu$, the information of d_m is critical.

Notice that if the value of j_c can be obtained at two different frequencies, denoted by j_{c1} and j_{c2}, combining Equations (5-6), (5-7) and (5-9) yields:

$$\ln j_{c1} - \ln j_{c2} = -\frac{\pi}{k_B T}\left(\frac{s\gamma_1^2}{\Delta\mu_1} - \frac{s\gamma_2^2}{\Delta\mu_2}\right) \tag{5-10}$$

Assume that the critical crystal nuclei are two-dimensional disks characterized by a radius r_c, then according to two-dimensional nucleation theory [9, 10]:

$$r_c = \frac{s\gamma}{\Delta\mu} \tag{5-11}$$

A combination of Equations (5-9), (5-10) and (5-11) yields:

$$F = B \ln d_m \tag{5-12}$$

$$F = \ln\frac{j_{c2}}{j_{c1}} + 2\frac{\pi}{s}\left(r_{c1}^2 \ln d_{01} - r_{c2}^2 \ln d_{02}\right), \qquad B = 2\frac{\pi}{s}\left(r_{c1}^2 - r_{c2}^2\right)$$

here d_{01}, d_{02} and r_{c1}, r_{c2} are the average distance d_0 and the critical size r_c measured in conditions producing j_{c1} and j_{c2} respectively. Experimentally, r_c can be evaluated from the critical size N^* with $\pi r_c^2 = N_{crys}^* \pi d_c^2$:

$$r_c = \frac{1}{2} d_c \sqrt{N_{crys}^*} \tag{5-13}$$

Because N_{crys}^*, d_0, d_c, j_c have been established as Figures 4.3(b), 5.1 and 5.2 show, d_m is the only unknown parameter in Equation (5-12), which can thus be derived from the slope of the plot F~B (Figure 5.3(a)). The result is $d_m \approx 1.28\,\mu m$.

Consequently, $\Delta\mu$ can be calculated by Equations (5-9) and the supersaturation σ for crystallization in the droplets can be calculated easily by $\ln(1+\sigma) = \Delta\mu / k_B T$. Since it is a simple algebra, the results of $\Delta\mu$ and σ are not presented.

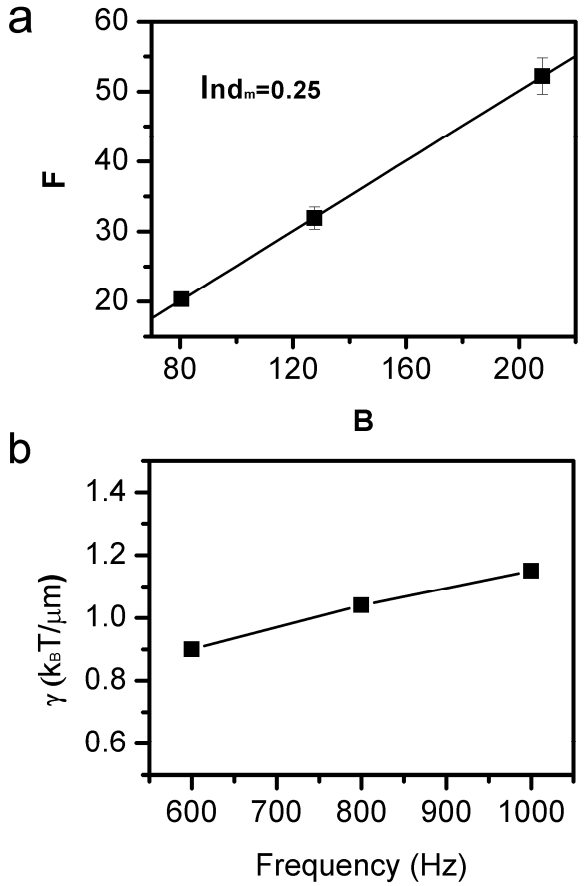

Figure 5.3 (a) F~B plot. The slope of a linear fit gives the value of $\ln d_m$. d_m is the equilibrium concentration in the amorphous precursor. (b) The calculated line tension or the interfacial free energy γ increases with frequency. The assumption of disk-like two-dimensional critical crystal nuclei leads to a high estimate of γ.

Given $d_m \approx 1.28\,\mu m$, γ can be calculated by combining Equations (5-9) and (5-11). The results for γ are shown in Figure 5.3(b). It is found that γ increases slightly with frequency. However, from Figure 5.2(b), we find that the distance d_c between two neighbor particles in the crystal nuclei does not change within the

frequency range we observe, indicating that the interaction between colloidal particles in the crystalline region does not change. It is expected that given the interaction, γ should be constant at a fixed temperature, contradicting with the results shown in Figure 5.3(b).

Notice that a key assumption contained in our calculation is that the shape of the critical crystal nuclei in the amorphous droplets is disk-like, characterized by the radius r_c. Given the critical size N^*_{crys}, this assumption leads to the minimum length of the crystal-liquid interface in the droplets. However, as can be seen in Figures 4.1(c) and 4.2(c), the shape of the crystal nuclei is normally irregular. Thus, the real length of the crystal-liquid interface is in fact much larger than that adopted in our calculation. Given the supersaturation and the nucleation energy barrier, the lower estimate of the interface length will result in a higher estimate of γ. Therefore, we conclude that the values shown in Figure 5.3(b) are much larger than the corresponding real values.

Moreover, as was discussed in Chapter 4, the change of the density and order degree in the droplets, from the crystalline core to the amorphous fringe, is continuous, making it easy for the colloidal particles residing on the crystal-liquid interface to become ‘crystal-like’ as well as ‘liquid-like’ via fluctuations. So, in our experiments, the shape of the crystals experiences large fluctuations from time to time due to the essentially local crystal-liquid transition at the interface. The fluctuations lead to a large divergence of the nucleus shape from the assumed disk-like. The stronger the

fluctuation, the larger the divergence between the real edge length and the estimated based on the disk-like assumption, and thus the bigger the error in the estimate of γ. Figure 5.2(b) reveals that as the frequency increases, the density in the amorphous region approaches that of the crystalline region. The reduced particle concentration difference between the crystalline region and its surrounding area enables the colloidal particles on the crystal edge to transform more easily between crystal-like and liquid-like. Consequently, the fluctuation of the crystal nucleus shape and thus the edge length becomes larger at high frequencies. It follows that the increase of γ with frequency may be attributed to the bigger errors contained in the calculation.

From the above discussion, it follows that in reality, γ should be smaller than the values shown in Figure 5.3(b). The experimental observations show that the irregular crystal edges are at least a factor two times the estimate obtained from the assumption that the crystal nuclei have a disk-like shape. It follows that the values of γ shown in Figure 5.3(b) are at least a factor two larger than their real values. Consequently, the real value of the interface free energy γ in the dense droplets should be less than $0.45 \sim 0.60\, k_B T / \mu m$.

5. 6 Conclusion

In this Chapter, a method is developed to calculate the local nucleation rate. Furthermore, the supersaturation and the interface free energy in the dense droplets are derived from the experimentally measured local nucleation rate. The continuous

change of the concentration in the dense droplets means a much lower interfacial free energy than estimated.

References

[1] P. R. ten Wolde and D. Frenkel, "Enhancement of Protein Crystal Nucleation by Critical Density Fluctuations," *Science*, vol. 277, pp. 1975-1978, 1997.

[2] V. Talanquer and D. W. Oxtoby, "Crystal nucleation in the presence of a metastable critical point," *J. Chem. Phys.* , vol. 109, pp. 223 1998.

[3] A. Shiryayev and J. D. Gunton, "Crystal nucleation for a model of globular proteins," *J. Chem. Phys.*, vol. 120, pp. 8318, 2004.

[4] C. Haas and J. Drenth, "The Interface between a Protein Crystal and an Aqueous Solution and Its Effects on Nucleation and Crystal Growth " *J. Phys. Chem. B* vol. 104, pp. 368, 2000.

[5] D. Kashchiev, P. G. Vekilov, and A. B. Kolomeisky, "Kinetics of two-step nucleation of crystals," *J. Chem. Phys.*, vol. 122, pp. 244706, 2005.

[6] P. G. Vekilov, "Dense Liquid Precursor for the Nucleation of Ordered Solid Phases from Solution," *Crys. Growth & Design*, vol. 4, pp. 671-685, 2004.

[7] Y. G. Kuznetsov, A. J. Malkin, and A. McPherson, "The liquid protein phase in crystallization: a case study-intact immunoglobulins," *J. Cryst. Growth*, vol. 232 pp. 30-39, 2001.

[8] X. Y. Liu, "From solid-fluid interfacial structure to nucleation kinetics: principles and strategies for micro/nanostructure engineering," in *Nanoscale Structure and Assembly at Solid-Fluid Interface*, vol. 1, X. Y. Liu and J. J. De Yoreo, Eds.: Kluwer Academic Publishers, 2004, pp. 109.

[9] D. Kashchiev, *Nucleation: Basic Theory with Applications*: Butterworth-Heinemann, Oxford, 2000.

[10] A. Laaksonen, V. Talanquer, and D. W. Oxtoby, "Nucleation: Measurements, theory, and atmospheric applications," *Annu. Rev. Phys. Chem.*, vol. 46, pp. 489, 1995.

Chapter 6 Effect of Long-Range Attraction on Growth Model

6. 1 Introduction

An important area of the study of crystallization is the atomistic processes underlying crystal growth. A major technological interest lies in the fabrication of crystalline thin films that are of fundamental importance in research and development of advanced electronic, optical, and magnetic materials which are the basis of modern technologies of computing and communication [1, 2]. The performance of thin films is essentially dependent on their surface morphology. Flat thin films are highly desirable in practice. However, growth of thin films is intrinsically a nonequilibrium process governed by a competition between kinetics and thermodynamics. The outcome of that growth is thus sensitive to a variety of atomic rate processes, and controlling these atomistic processes is crucial in developing high quality thin films.

Especially as the dimension of devices has shrunk to the nanometer scale, precise control at the atomic scale becomes critical. However, this sort of control is experimentally inaccessible without a full understanding of the mechanisms underlying atomistic processes.

Experimentally, the temperature is one of the most important parameters in controlling thin film growth. Therefore, much attention has been focused on exploring the effect of temperature on the outcome of thin film growth [3-6]. To achieve flat thin films, two-dimensional (2D) growth, the so-called layer-by-layer growth, is desired. Due to the step-edge barrier, namely the Ehrlich-Schwoebel (ES) barrier, (2D) growth usually occurs at high temperatures [6]. Decreasing the temperature leads to a three-dimensional (3D) growth, and thus a rough surface [6, 7]. Nevertheless, it has been found that at some low temperatures, 2D instead of 3D growth occurs [8]. The reentrant 2D growth at low temperatures is the most intriguing phenomenon found in thin film growth

To understand 2D growth occurring at low temperatures, atomistic models were built [6, 9]. In these models, downward funneling (DF) was supposed to be an important mechanism underlying the reentrant smooth growth [9-11]. According to DF, atoms deposited beyond a step edge would tend to funnel down to the lower layers due to their condensation energy. At high temperatures, the effect of DF on the growth is negligible while it becomes significant at low temperatures when the size of the islands or mounds becomes small.

Recent studies, however, revealed that due to the attraction between steps and incoming atoms, incoming atoms will be preferentially collected by the top layers of the islands and mounds. This effect is known as “steering effect” [12-14]. The discovery of the steering effect poses a great challenge to the mechanism of DF. It was found that due to the steering effect, the incoming atoms beyond the step edges are preferentially attracted to the uppermost layers rather than funnel down to the lower layers as suggested by DF [15]. Thus, the steering effect tends to undermine the effect of DF. The following question arises: if DF cannot support a 2D growth at low temperatures due to the step-adatom attraction, what is the underlying mechanism of the reentrant 2D growth?

Notice that in most previous works, the studies of the steering effect and DF were based on computer simulations in which experimental conditions were considerably simplified and the interplay between different atomistic processes was customarily neglected. However, in real experiments, thin film growth is a nonequlibrium process consisting of a variety of different atomistic processes. Generally, a specific growth model is an outcome of the interplay between different atomistic processes. For example, experimentally, there should always be some adatoms diffusing on the terraces or along the step edges. Therefore, given that the attraction between steps and incoming atoms can modify the trajectories of the incoming atoms, this attraction should also affect the behavior of the adatoms diffusing near step edges. However, to study this effect, direct observation of the motion of the individual atoms is necessary.

In this study, the growth model is studied in our colloidal model system where colloidal particles interact through a long-range attraction.

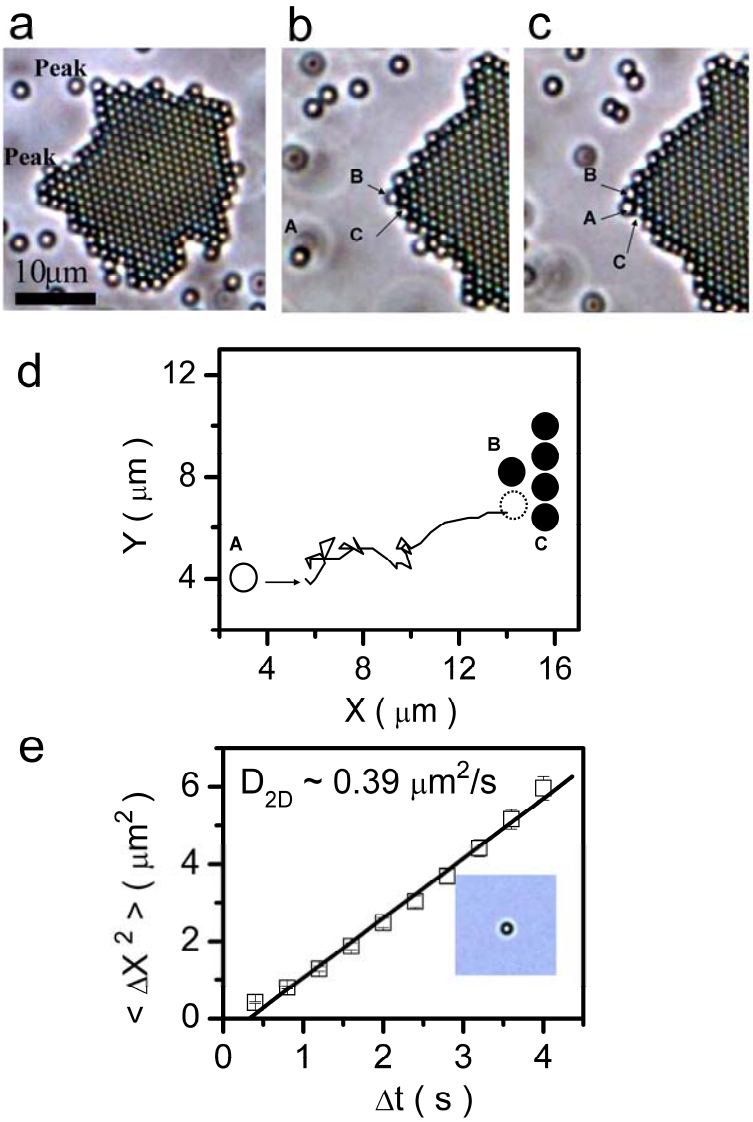

Figure 6.1 Steering effect induced by attraction: (a) Step protrusions on the growing front. (b)-(c) Incorporation process of particles A. (d) Trajectory of particle A. (e) The two-dimensional diffusion coefficient of colloidal particles on the glass substrate.

6. 2 Growth Models Induced by Attraction

6. 2. 1 Steering Effect

An intriguing phenomenon in our experiments is that the growing 2D crystals are usually characterized by step protrusions as shown in Figure 6.1(a). However, colloidal particles in this system are homogeneously transported to the growing crystals. The formation of step protrusions indicates that the approaching particles are directed preferentially by a force into the peaks of the step protrusions. To identify the mechanism underlying the formation of step protrusions, hundreds of incorporation processes of incoming particles are investigated individually.

Snapshots shown in Figures 6.1(b)-(c) illustrate a typical incorporation process at the peak of a step protrusion. In Figure 6.1(b), a particle A is approaching the growing crystal. In Figure 6.1(c), particle A eventually becomes incorporated at the peak of the protrusion. The trajectory of particle A is recorded and shown in Figure 6.1(d) which shows that particle A experiences two distinct motions in succession while approaching the step protrusion. Firstly, it undergoes a Brownian motion. The Brownian motion comes to an end when particle A is about 5 μm away from the step protrusion. Subsequently, the particle follows a direct motion along a straight line toward the peak of the step protrusion. It is clear from Figure 6.1(d) that the Brownian motion of particle A shows no tendency to diffuse towards the step protrusion. It is the following well-directed straight motion which transports particle A to the peak of the step protrusion. The well-directed straight motion suggests that there should exist

an attraction between particle A and the growing protrusion. The distance traveled along the straight line offers a good quantitative measure of the working range of the attractive force. In our experiments, the average length of the straight trajectory is measured at $5 \sim 6\,\mu m$ which, compared with the diameter $1\,\mu m$ of the colloidal particles, is long-range.

To be sure that the behavior of particle A is not induced by the interaction between the colloidal particles and the glass substrate, the two-dimensional diffusion coefficient D_{2D} of the colloidal particles far away from the growing crystals was calculated by measuring the mean square displacement $\langle \Delta x^2 \rangle$ of a diffusing particle as a function of the investigated interval Δt. D_{2D} is determined from the slope of the linear fit of $\langle \Delta x^2 \rangle \sim \Delta t$ which gives $D_{2D} = \langle \Delta x^2 \rangle / 4\Delta t = 0.39 \pm 0.02\ \mu m^2/s$. . According to the Stokes-Einstein equation, the diffusion coefficient can also be calculated by:

$$D = \frac{kT}{6\pi\eta R} \tag{6.1}$$

In our case, T is $293K$, the corresponding water viscosity $\eta(T)$ is given by $10^{-3} Nsm^{-2}$ and the particle radius R is $0.5\,\mu m$. Thus, the theoretical diffusion coefficient is given by $0.43\ \mu m^2/s$. This is slightly higher than that obtained experimentally. However, near the glass wall, hydrodynamic effect will give rise to a water viscosity which is larger than the normal value. Taking this into consideration, we may explain the slight discrepancy between the experimentally measured D and the theoretical estimated D. From the above discussion, we conclude that our experimental

measurement is convincing within the available margin of uncertainty, and most importantly, it follows that the ITO glass surface has little effect on the behavior of the colloidal particles. Therefore, the straight motion of particle A as shown in Figure 6.1(d) is very likely a result of the attractive interaction between it and the step protrusion.

Further confirmation of the existence of that attraction comes from the acceleration of the incoming particles when they approach the step protrusions. Given the diffusion coefficient D_{2D}, the free diffusion velocity of colloidal particles can be determined by:

$$V_{2D} = <\Delta x>_{\Delta t = 1s} = \sqrt{4D_{2D}} \tag{6.2}$$

The result is ~ 1.25 $\mu m/s$. The velocity just prior to the impingement on the steps is measured and averaged over hundreds of particles. The result is ~3.69 $\mu m/s$. It is clear that incoming particles are strongly accelerated as they approach the steps, offering direct evidence of the attractive force working between the incoming particles and the step particles.

From the above discussion, one can conclude that the well-directed straight motion of particle A in Figure 6.1 is caused by the attraction between the incoming particles and the step particles. The incorporation process of particle A also suggests that because of the attraction, incoming particles will be collected preferentially by the peaks of the step protrusions, giving rise to a growth instability which in turn promotes the growth of the step protrusions. This result is consistent with previous

studies of the steering effect [14, 15]. Here the long-range attraction is between the incoming particles and the step is induced by EHD mechanism as we have introduced in 2.3. This kind of mechanism is different from that working between atoms as we will discuss in 6.3.

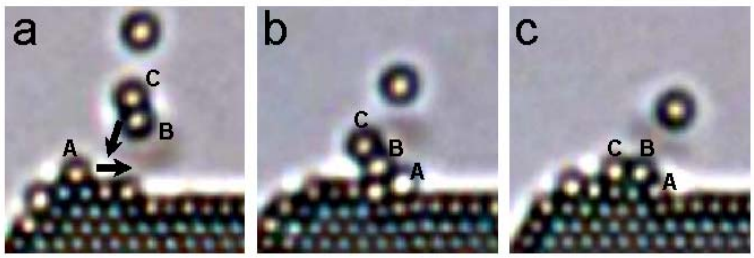

Figure 6.2 Descending transport triggered by the attraction from the incoming dimer.

6. 2. 2 Interlayer Transport

The steering effect, however, reflects only one aspect of the consequences of the attraction between incoming particles and step particles. In previous simulations, the consequence of the attractive force exerted by incoming particles on the particles diffusing near step edges was neglected. Furthermore, it was assumed in simulations that incoming atoms approach the step one by one. However, this does not hold true in real experiments. In practice, incoming units can be dimers, trimers, and even larger clusters of growth units. The larger the incoming units, the stronger the attractive force felt by the particles diffusing near step edges.

In Figure 6.2(a), an adsorbed monomer A stays on a growing front as one dimer consisting of particles *B* and *C* is approaching. As the dimer moves close to the step within a distance of about several particle diameters, the attraction from the dimer begins to accelerate particle A (Figure 6.2(b)) and eventually gets it down to the lower layer (Figure 6.2(c)). This process illustrates that it is possible for the attraction from the incoming clusters to induce an additional interlayer transport.

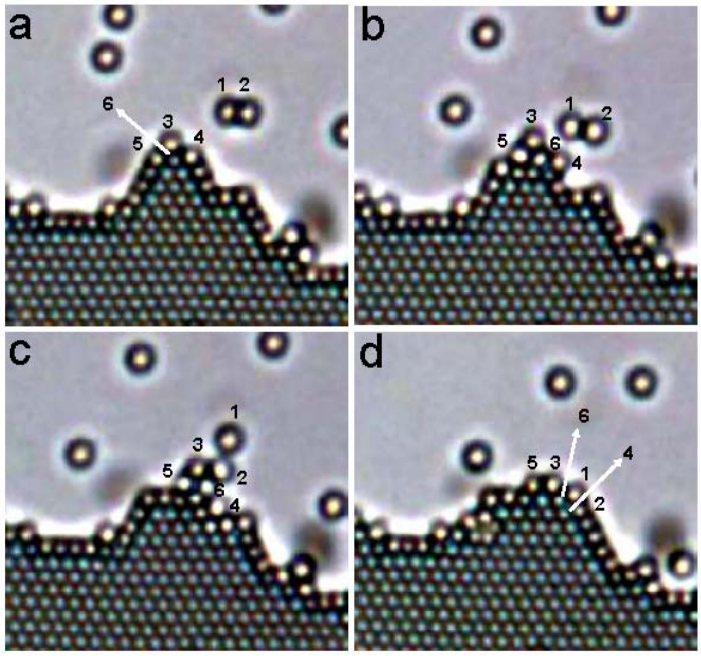

Figure 6.3 Smoothing effect of the attraction: (a)-(d): Step particles are pulled down to the lower layers by incoming dimmers, resulting in a reduction of the local roughness.

The process presented in Figure 6.2 is the simplest case in our experiments. Figure 6.3 shows a more complicated but more widespread process in our experiments. In Figure 6.3(a), particles numbered 3-6 form the peak of the step protrusion, and an

incoming dimer consisting of particles 1 and 2 is approaching the peak. When the incoming dimer is close enough to interact with the peak, its trajectory is directed towards the step peak (Figure 6.3(b)). At the same time, particles 3-6 begin to move due to the attraction from the incoming dimer. At the end of this process, particles 4 and 6 are finally pulled down to the lower layers (Figure 6.3(c)-(d)), and the incoming dimer also becomes incorporated into the peak. As a result of this process, the peak becomes smoother and it is widened so as to be able to accept more incoming particles. This attraction-induced smoothing effect has never been suggested in previous studies, but it does occur in our experiments.

From the above discussion, we find that the role of the attraction between the incoming particles and the growing front is twofold: it can induce the steering effect as well as the smoothing effect. The steering effect leads to the creation of step protrusions by attracting incoming particles to the uppermost layers while the smoothing effect gets part of the adsorbed particles down the lower layers. The attraction-induced smoothing effect works effectively in smoothening out the local growing front as Figure 6.4(a)-(c) shows. However, the long-term consequence of the attraction is illustrated by Figure 6.4(d): global step protrusions are created when the local small step protrusions are smoothened out during the growth. However, it is clear that the long-term consequence can become obvious only when the growth lasts a relatively long time. In thin film growth, to observe the global step protrusions, the thickness of the film has to be larger than a certain value.

The smoothing effect of the attraction was not discovered in previous studies[13-15] because the influence of the attraction from incoming adatoms on the adsorbed adatoms was not considered overall comprehensively. That attraction was considered only as a mechanism for producing the growth instability and enhancing mound formation. Based on our experimental results, we conclude that incomplete understanding was reached in previous studies.

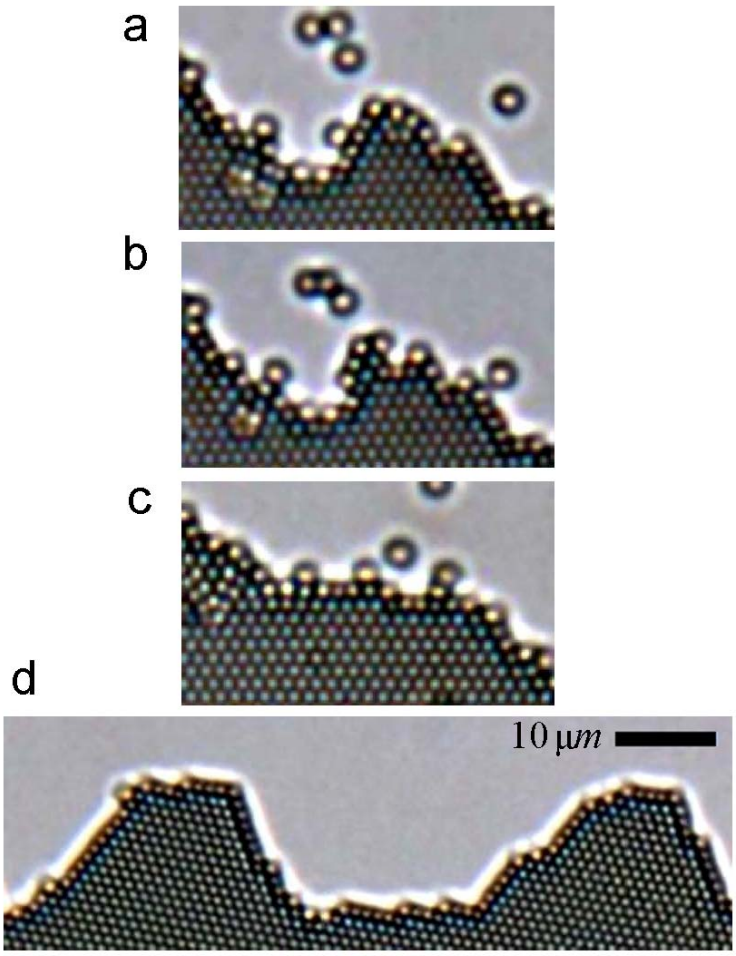

Figure 6.4 Interplay between the steering effect and the smoothing effect: (a)-(c) The gap between two neighbor small step peaks is filled up by the descending transport induced by the attraction. (d) The long-term consequence of the attraction is represented by the global step protrusions.

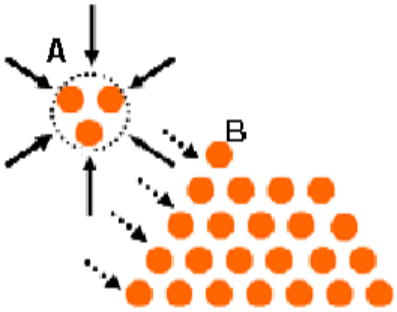

Figure 6.5 EHD-induced attraction between the incoming clusters and the step particles: The attraction induced by EHD mechanism between a step particle and an incoming clusters will be weakened by fluid flow induced by other step particles. Solid arrow: direction of the fluid flow induced by incoming clusters A. Dashed arrow: direction of the fluid flow induced by step colloidal particles.

6. 3 Effect of the Nature of Attraction

The long-range attraction between colloidal particles in our experiments is different by nature from that acting between atoms. In the case of atoms, the attraction originates directly from other atoms, while the long-range attraction between colloidal particles here proceeds through fluid flow, and hence the range of the long-range attraction is determined by the scale of the fluid flows. It was found that the scale of the fluid flows around colloidal particles or clusters is frequency-dependent [16]. Given the scale of fluid flow, incoming particles are preferentially captured by the fluid flow induced by step protrusions. Therefore, the role of fluid flow in bringing colloidal particles together to form crystals and in producing the steering effect can be represented by an attractive force F_h. Nadal et al. suggested that F_h can be

approximated by the Stoke's force: $F_h \sim 6\pi\eta\, a\, u(r,\omega)$, where a is the radius of the colloidal particle, η is the viscosity of the solvent. According to Nadal et al. the fluid velocity $u(r,\omega)$ at a distance r from the center of the colloidal particle is frequency dependent, giving $r >> a$:

$$< u(r,\omega) >_t = V_a A_a e^{-r/l(\omega)} \tag{6.3}$$

where $l(\omega)$ is the frequency dependent characteristic length of the fluid flow which is induced by the presence of the charged colloidal particles. Both V_a and A_a are frequency-dependent constants. For $r >> l(\omega)$, $u(r,\omega)$ decreases as $1/r^3$.

Formally, F_h is distinct from the attractions used in simulations based on potentials like the Lennard-Jones (LJ) potential [13, 15] or the Embedded Atom Method (EAM) potential [14, 15]. However, by comparing the results of the LJ potential and the EAM potentials Yu et al.[15] found out that the degree of the steering effect does not strongly depend on the details of the interaction potential. However, increasing the cutoff distance of the LJ interaction potential can enhance the steering effect. This means that the most important parameter in the steering effect is the range of the attraction. The range of F_h in this study is estimated as about 5~6 times the diameter of the colloidal particles, much larger than that employed in simulations. This suggests that the steering effect in our experiments should be stronger than that in typical atomic systems.

The most interesting phenomenon observed in our experiments is the smoothing effect induced by F_h during the growth of the colloidal crystals. The question is

whether this result is applicable in typical atomic systems. In atomic systems, the attractive force exerted by an incoming cluster on a step atom is independent of the existence of other step atoms. However, in our system, the attractive force F_h of the incoming clusters has to be exerted on a step particle through fluid flows as Figure 6.5 shows. When the incoming clusters approach the steps, the fluid flow around them will be disturbed and usually weakened by the fluid flows induced by other step atoms. Therefore, the final attractive force exerted by incoming cluster A on step particle B (Figure 6.5) should be smaller than that indicated by F_h. At this point, we suggest that direct attractions in atomic systems should be more effective than the attraction caused by the EHD mechanism in inducing the smoothing effect.

Here, the smoothing effect of the attraction discovered in our experiments offers a mechanism which may contribute to the reentrant smooth growth observed in epitaxial growth at low temperatures [8]. It is obvious that the smoothing effect of the attraction will be promoted when step protrusions become smaller so that the particles adsorbed on the top of the step protrusions can be more easily reached by the attraction from the incoming clusters. This effect makes it more likely that the absorbed particles will be pulled down to the lower layers. This condition is well satisfied in the epitaxial growth conducted at low temperatures. According to the nucleation theory, more and smaller islands will be nucleated at low temperatures on the growing surface because of the reduced mobility of adatoms. The reduced mobility of adatoms causes them to remain near where they landed. Therefore, the

adatoms collected through the steering effect stay near the step edges and are especially amenable to being pulled down by the attraction from incoming clusters. At this point, the epitaxial growth proceeding at low temperatures offers a good environment for the attraction-induced smoothing effect to work.

Nevertheless, also the strength of the attraction from the incoming clusters plays an important role in the smoothing effect. As we have seen in Figure 6.1, incoming monomers are not likely to induce an interlayer transport due to their small attraction to the step adatoms. On the other hand, the incorporation of incoming dimers is often accompanied by an interlayer transport because of the stronger attraction exerted on the step particles. At this point, we argue that a certain number of dimers or bigger incident clusters can promote the occurrence of flat thin films at low temperatures.

Another important factor which may affect the smoothing effect is the attraction between colloidal particles inside crystals, which, we believe, is different in mechanism from EHD. In fact, it has been experimentally investigated that the fluid flow which contributes greatly into the EHD-induced attraction becomes every weak in the clusters, and is not strong enough to support the short-range attraction working between colloidal particles inside the crystals [17]. However, to the best of our knowledge, there has so far no experimental and theoretical work to discuss the possible mechanism underlying the short-range attraction. Therefore, it is difficult currently to discuss even qualitatively the effect of the short-range attraction on the smoothing effect.

6. 4 Conclusions

We find that the attraction between the incoming clusters and the growing fronts can induce an additional interlayer transport as well as generate the steering effect. This observation suggests that when the DF mechanism is suppressed by the occurrence of the steering effect, the attraction-induced interlayer transport also contributes a mechanism allowing adatoms to descend, thus leading to a smoothening effect. Of course, whether this kind of mechanism is strong enough to replace the role of DF in the 2D growth is still open to question. We suggest that in future simulations, in addition to the steering effect, also the influence of the attraction exerted by incoming clusters on the existing adatoms near the step edges should be taken into consideration.

References

[1] S. Park, B. L. Clark, D. A. Keszler, J. P. Bender, J. F. Wager, T. A. Reynolds, and G. S. Herman, "Low-Temperature Thin-Film Deposition and Crystallization," *Science*, vol. 297, pp. 65, 2002.

[2] K. Sieradzki, S. R. Brankovic, and N. Dimitrov, "Electrochemical Defect-Mediated Thin-Film Growth," *Science*, vol. 284, pp. 138, 1999.

[3] J. Jacobsen, K. W. Jacobsen, P. Stoltze, and J. K. Nørskov, "Island shape-induced transition from 2D to 3D growth for Pt/Pt(111)," *Phys. ReV. Lett.* , vol. 74, pp. 2295, 1995.

[4] I.-S. Hwang, S.-H. Chang, L.-J. Chen, and T. T. Tsong, "Observation of Finite-Size Effects on a Structural Phase Transition of 2D Nanoislands," *Phys. Rev. Lett.* , vol. 93, pp. 106101, 2004.

[5] E. Cox, M. Li, P.-W. Chung, C. Ghosh, T. S. Rahman, C. J. Jenks, J. W. Evans, and P. A. Thiel, "Temperature dependence of island growth shapes during submonolayer deposition of Ag on Ag(111)," *Phys. Rev. B* vol. 71, pp. 115414, 2005.

[6] H. Jónsson, "Theoretical Studies of Atomic Scale Processes Relevant to Crystal Growth," *Annu. ReV. Phys. Chem.* , vol. 51, pp. 623, 2003.

[7] C. R. Stoldt, K. J. Caspersen, M. C. Bartelt, C. J. Jenks, J. W. Evans, and P. A. Thiel, "Using Temperature to Tune Film Roughness: Nonintuitive Behavior in a Simple System," *Phys. Rev. Lett.*, vol. 85, pp. 800, 2000.

[8] R. Kunkel, B. Poelsema, L. K. Verheij, and G. Comsa, "Reentrant layer-by-layer growth during molecular-beam epitaxy of metal-on-metal substrates " *Phys. Rev. Lett.* , vol. 65, pp. 733, 1990.

[9] K. J. Caspersen, C. R. Stoldt, A. R. Layson, M. C. Bartelt, P. A. Thiel, and J. W. Evans, "Morphology of multilayer Ag/Ag(100) films versus deposition temperature: STM analysis and atomistic lattice-gas modeling " *Phys. Rev. B*, vol. 63, pp. 085401, 2001.

[10] M. Li and J. W. Evans, "Theoretical Analysis of Mound Slope Selection during Unstable Multilayer Growth," *Phys. Rev. Lett.*, vol. 95, pp. 256101, 2005.

[11] M. Biehl, "Lattice gas models and Kinetic Monte Carlo simulations of epitaxial growth " in *Multiscale Modeling in Epitaxial Growth*, vol. 149, *Int. Series of Numerical Mathematics* A. Voigt, Ed. Basel, Switzerland: Birkhaeuser, 2005, pp. 3.

[12] S. C. Wang and G. Ehrlich, "Adatom motion to lattice steps: A direct view " *Phys. Rev. Lett.*, vol. 70, pp. 41, 1993.

[13] S. van Dijken, L. C. Jorritsma, and B. Poelsema, "Steering-Enhanced Roughening during Metal Deposition at Grazing Incidence " *Phys. Rev. Lett.*, vol. 82, pp. 4038, 1999.

[14] F. Montalenti, M. R. Sørensen, and A. F. Voter, "Closing the Gap between Experiment and Theory: Crystal Growth by Temperature Accelerated Dynamics " *Phys. Rev. Lett.*, vol. 87, pp. 126101, 2001.

[15] J. Yu and J. G. Amar, "Effects of Short-Range Attraction in Metal Epitaxial Growth " *Phys. Rev. Lett.*, vol. 89, pp. 286103, 2002.

[16] F. Nadal, F. Argoul, P. Kestener, B. Pouligny, C. Ybert, and A. Ajdari, "Electrically induced flows in the vicinity of a dielectric stripe on a conducting plane " *Eur. Phys. J. E* vol. 9, pp. 387, 2002.

[17] J. Santana-Solano, D. T. Wu, and D. W. M. Marr, "Direct Measurement of Colloidal Particle Rotation and Field Dependence in Alternating Current Electrohydrodynamic Flows" *Langmuir vol. 22, pp. 5932, 2006.*

Chapter 7 Properties of Point Defects

7.1 Introduction

The solid state is one of the most important states of matter. Most solids are crystalline in structure. Crystalline solids are widely used in fabricating advanced materials due to their special electronic, optical, and magnetic properties. However, most real crystalline solids are not perfect, containing a number of defects. According to their dimensionality, defects can be classified into three types: point defects, one-dimensional defects, and two-dimensional defects [1]. A point defect means that a single atomic site, or a complex consisting of a few atomic sites is not in the proper crystalline positions. The most important point defects are vacancies and interstitials. In a vacancy, one or a few atoms are missing, while in interstitials, extra atoms are present. One-dimensional defects are dislocations that consist of lines of atomic sites dislocated from their ideal positions. Typical two-dimensional defects are the so-called grain boundaries that are the intersections between two crystallites.

Defects have a profound impact on the performance of materials. For example, dislocations can influence their electrical and optical properties [2, 3]; vacancies in solids facilitate diffusion. Recent studies further revealed that vacancies in graphene layers strongly influence the physical and chemical properties of carbon nanostructures [4, 5]. Therefore, defect dynamics is of great importance in both condensed-matter physics and materials science. However, direct observations of defects in atomic materials are difficult. As an alternative approach, colloidal crystals have been employed as model systems in the past few years for the study of defect properties [6-10]. These studies have offered plenty of insight and shed light on our understanding of defect dynamics.

It is found, however, that in previous studies [6, 8-10], the interactions between colloidal particles are usually taken to be purely repulsive. Then, the question arises: are the results obtained in these studies applicable in real atomic materials in which atoms interact through attractive forces? No such study on colloidal crystals has been conducted to address this question. However, this kind of study is of great importance for both fundamental physics and technological applications. The reason is that introducing a specific attraction into a colloidal system can offer a robust strategy for producing photonic-band-gap materials [11]. The aim of this work is to study the configuration and diffusion of vacancies in our two-dimensional colloidal model system in which a long-range attraction works between colloidal particles. In this system, the attractive interaction potential between colloidal particles is similar in

shape to that acting in typical atomic systems [12]. It is found that the dynamics of defects observed in our experiments is distinct from previous observations where the interaction between colloidal particles were taken to be purely repulsive [9, 10].

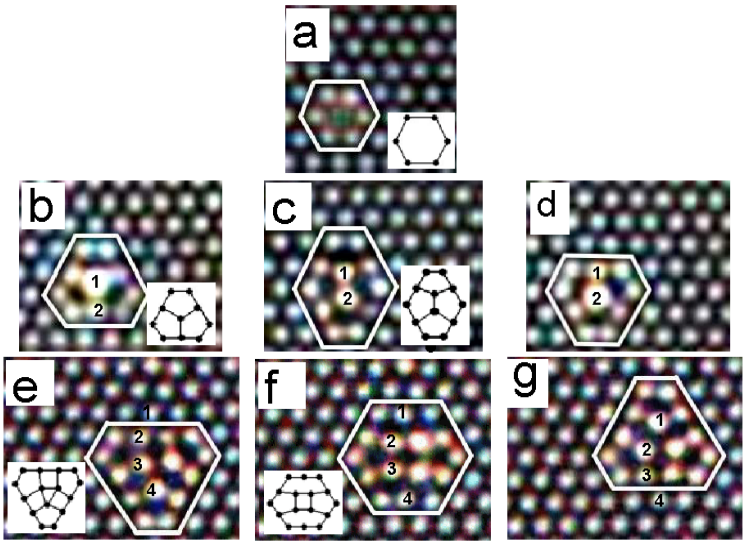

Figure 7.1 Configuration of vacancies: (a) Monomer vacancy with symmetry D_6. Configurations of dimer vacancy: (b) threefold symmetric D_3; (c) twofold symmetric D_2. Configurations of trimer vacancy: (e) threefold symmetric D_3; (f) twofold symmetric D_2. Time sequences (b)-(d) and (e)-(f) illustrate how dimer vacancies and trimer vacancies diffuse in crystals.

7. 2 Configurations of Vacancies

Monomer vacancies in our experiments are immobile and cannot diffuse within the crystals. The topological structure of monomer vacancies is invariant and exhibits identical symmetry to the underlying hexagonal lattice (Figure 7.1(a)). However, monomer vacancies in systems dominated by purely repulsive interactions descend into some configurations with reduced symmetry in comparison with the underlying hexagonal lattice [9, 10, 13]. On the other hand, there are two configurations in our

experiments for dimer vacancies as Figures 7.1(b)-(c) show. Trimer vacancies exhibit also two configurations as shown in Figure 7.1(e)-(f). The dimer vacancy in Figure7.1(b) and the trimer vacancy in Figure 7.1(e) are threefold symmetric (D_3). The dimer vacancy in Figure 7.1(c) and the trimer vacancy in Figure 7.1(f) are twofold symmetric (D_2).

To identify the occurrence probability of the configurations, one thousand of pictures are taken with an interval 0.2s for every defect. We find that the transition from one configuration to another configuration is very fast (<0.1s). Therefore, 0.2s is enough for defects to reach equilibrium. For dimer vacancies, we found that there are about 470 pictures in which the dimer vacancy adopts the configuration with symmetry D_2. Therefore, the relative occurrence probabilities of D_2 and D_3 for dimmer vacancies are identified as 0.47 ± 0.01 and 0.53 ± 0.01 respectively. The probability of D_3 is only slightly higher than that of D_2. The occurrence probability P of a specific configuration is dependent on its occupation energy ε by:

$$P = A\exp(-\varepsilon / k_B T) \tag{7.1}$$

The free energy difference $\Delta\varepsilon$ (which is determined by the interaction potential) between dimer vacancies with symmetry D_2 and D_3 respectively can be estimated from the occurrence probabilities. The calculation shows that $\Delta\varepsilon$ is about 0.12 $k_B T$. For trimer vacancies, the relative occurrence probability for D_3 is 0.68 ± 0.01 which is significantly higher than 0.32 ± 0.01 for D_2, that is, trimer vacancies with higher symmetry are in our experiments more stable. The occupation energy of trimer

vacancies with symmetry D_2 is higher than that with symmetry D_3 by 0.75 k_BT.

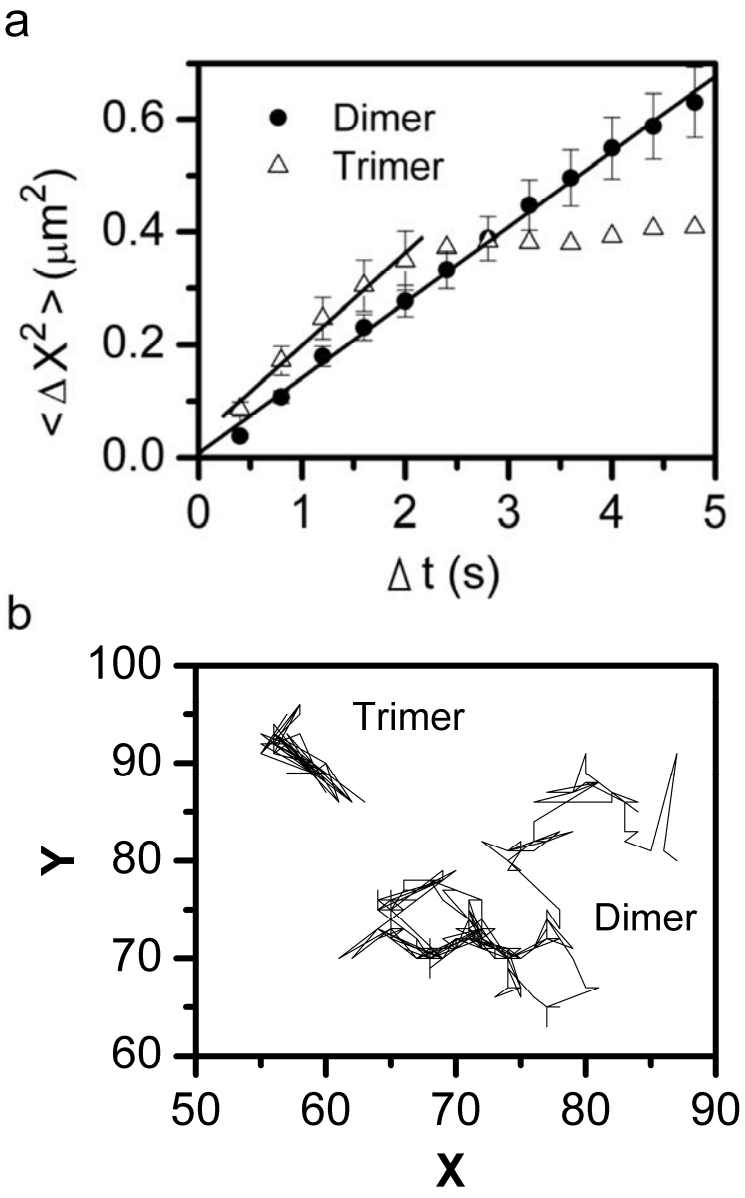

Figure 7.2 Diffusion of vacancies: (a) Average squared displacement of vacancies as function of the time separation. (b) Trajectories of vacancies.

7.3 Diffusion of Vacancies

Diffusivity is another important property of defects. As we mentioned above, monomer vacancies are immobile in our system. The diffusion route of dimer vacancies is illustrated by the time sequence Figure 7.1(b)-(d). Originally, particle 1 stays at the defect center balanced by the attractions from surrounding particles (Figure 7.1(b)). Thermal fluctuations cause particle 1 to leave its equilibrium position, and subsequently the attraction between particle 1 and particle 2 pulls particle 2 into the vacancy interior (Figure 7.1(c)). From the configuration as shown in Figure 7.1(c), the dimer vacancy can hop back to its original position with particle 1 at the center (Figure 7.1(b)) or hop to another neighbor site (Figure 7.1(d)) with particle 2 now at the defect center, which leads to an effective walk of the dimer vacancy. The topological structures of the dimer vacancy in Figure 7.1(b) and Figure 7.1(d) are identical, but the defect center undergoes a migration of $\sim 0.6 r_{eq}$ from Figure 7.1(b) and Figure 7.1(d). The diffusion route of trimer vacancies is similar to dimer vacancies as Figure 7.1(e)-(g) show, but more particles are involved. The average of the positions of 5-fold-coordinated particles around the vacancy core is defined as position (*x)* of the vacancies [9]. The positions of the vacancies as a function of time in our experiments are identified from the recorded continuous frames. The average squared displacements $<\Delta x^2>$ are plotted as a function of the time separation Δt (Figure 7.2(a)). The relationships between $<\Delta x^2>$ and Δt are then linearly fit. From the slopes of the linear fits, the diffusion coefficients of the vacancies are calculated

by $D = \frac{\langle \Delta x^2 \rangle}{4\Delta t}$. The diffusion coefficient of the dimer vacancies D_{di} is measured at $0.13 \pm 0.03\ \mu m^2/s$.

Nevertheless, the average squared displacements $< \Delta x^2 >$ of trimer vacancies stop increasing when the time separation exceeds 2*s* (Figure 7.2(a)). This means that the motion of trimer vacancies is limited within a subregion. Because the relative occurrence probability of symmetry D_3 (0.68) is significantly higher than that of D_2 symmetry (0.32), the trimer vacancies stay in the threefold symmetric configuration (Figure 7.1(e)) most of the time. Occasionally, they hop to their twofold symmetric configuration, resulting in a rearrangement of the colloidal particles (Figure 7.1(f)). The trimer vacancy in Figure 7.1(f) will either hop back to its original position (Figure 7.1(e)) or soon hop to a different position (Figure 7.1(g)). In the case of dimer vacancies, these two tendencies occur with the same probability. However, detailed observations reveal that trimer vacancies exhibit a strong tendency to hop back to their initial positions (From Figure 7.1(f) to Figure 7.1(e)) with a relative probability 0.90. Therefore, trimer vacancies in our experiments undergo mainly local vibrations between their two configurations instead of undergoing a global diffusion. A similar observation has been reported and discussed in a previous study [9] which supposed that during hopping, colloidal particles in the defect core can rearrange themselves rapidly. Because the lattice around the core cannot respond as fast as the core region, eventually the defect is pulled back to its initial site. The relaxation response of the lattice to the distortion produced by the fast rearrangement of the defect core will

become slower when vacancies are larger. Consequently more lattice particles will become involved in the hopping. For that reason, the global diffusion of vacancy clusters, such as trimer vacancies and tetramer vacancies, is normally inhibited. The local oscillation of trimer vacancies is well reflected by the trajectories of the core of a trimer vacancy (Figure 7.2(b)). The trajectories of dimer vacancies are typically a global Brownian motion shown in Figure 7.2(b).

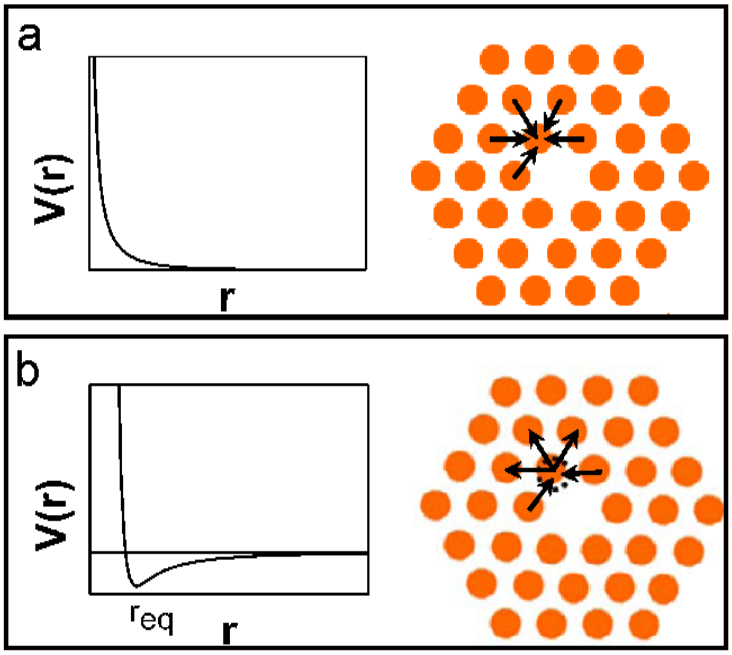

Figure 7.3 Effect of interaction on properties of vacancies: (a) In a system governed pure repulsion, particles next to the missing particle of a monomer vacancy tend to be pushed towards the vacancy center. (b) The tendency of particles next to the missing particle of a monomer vacancy to move towards the vacancy center is inhibited by the strong recovering force.

7. 3 Effect of Interaction on Properties of Vacancies

In previous studies [9, 10], monomer vacancies exhibit several different configurations with reduced symmetry and they can diffuse as fast as dimer vacancies. Especially, configurations with higher symmetry are not the most stable. Furthermore, dimer vacancies can dissociate into a dislocation pair. All these observations diverge significantly from our observations. These discrepancies, in our opinion, arise from the difference in the nature of the interaction. In colloidal crystals, dominated by purely repulsive forces [9, 10], the direction of the net force acting on the particles adjacent to the missing particle of monomer vacancies points towards the vacancy center as Figure 7.3(a) shows. Therefore, particles next to the missing particle are pushed toward the vacancy center, resulting in deformation and diffusion of monomer vacancies. However, in our experiments, the electrostatic repulsion between two nearest neighbor colloidal particles inside the clusters is balanced by an attraction at an equilibrium center-to-center distance r_{eq} [14-17], namely the lattice constant. Therefore, inside the clusters, the shape of the effective interaction potential around r_{eq} can be depicted by the curve in Figure 7.3(b). A small deviation of colloidal particles from their equilibrium positions produces a recovering force to pull them back (Figure 7.3(b)). Therefore, the hopping of colloidal particles next to the missing particles of monomer vacancies is strongly inhibited by the recovering force (Figure 7.3(b)). A recent observation has suggested that monomer vacancies in graphene layers are actually immobile in normal conditions [18] and in simulations[19], the

diffusion of monomer vacancies is active only at high temperatures ($> 3000K$).

In summary, our observations reveal that the nature of the interaction acting between colloidal particles has a significant impact on the configurations and the diffusion of defects. Our results presented in this thesis offer a further understanding of the defect dynamics which is applicable in atomic materials as well as in colloid crystals.

References

[1] E. Kaxiras, *Atomic and Eletronic Structure of Solids*: Cambridge University Press, 2003.

[2] S. Mrowec, *Defects and Diffusion in Solids: An Introduction*: Elsevier, New York, 1980.

[3] R. J. D. Tilley, *Principles and Applications of Chemical Defects*: Stanley Thornes Ltd., Chettenham, 1998.

[4] A. Hansson, M. Paulsson, and S. Stafström, "Effect of bending and vacancies on the conductance of carbon nanotubes " *Phys. Rev. B*, vol. 62, pp. 7039, 2000.

[5] C. P. Ewels, M. I. Heggie, and P. R. Briddon, "Adatoms and nanoengineering of carbon," *Chem. Phys. Lett.* , vol. 351 pp. 178, 2002.

[6] P. Lipowsky, M. J. Bowick, J. H. Meinke, D. R. Nelson, and A. R. Bausch, "Direct visualization of dislocation dynamics in grain-boundary scars," *Nature Mat.*, vol. 4, pp. 407, 2005.

[7] P. Schall, I. Cohen, D. A. Weitz, and F. Spaepen, "Visualizing dislocation nucleation by indenting colloidal crystals," *Nature*, vol. 440, pp. 319, 2006.

[8] C. Eisenmann, U. Gasser, P. Keim, G. Maret, and H. H. von Grünberg, "Pair Interaction of Dislocations in Two-Dimensional Crystals," *Phys. Rev. Lett.*, vol. 95, pp. 185502, 2005.

[9] A. Pertsinidis and X. S. Ling, "Diffusion of Point Defects in Two-Dimensional Colloidal Crystals," *Nature*, vol. 413, pp. 147, 2001.

[10] A. Pertsinidis and X. S. Ling, "Equilibrium Configurations and Energetics of Point Defects in Two-Dimensional Colloidal Crystals " *Phys. Rev. Lett. 87*, vol. 87, pp. 098303, 2001.

[11] P. Bartlett and A. I. Campbell, "Three-Dimensional Binary Superlattices of Oppositely Charged Colloids," *Phys. Rev. Lett.* , vol. 95, pp. 128302, 2005.

[12] T. M. Squires and M. P. Brenner, "Like-charge attraction through hydrodynamic interaction," *Phys. Rev. Lett.* . , vol. 85, pp. 4976, 2000.

[13] S. Jain and D. R. Nelson, "Statistical mechanics of vacancy and interstitial strings in hexagonal columnar crystals " *Phys. Rev. E*, vol. 61, pp. 1599, 2000.

[14] M. Trau, D. A. Saville, and I. A. Aksay, "Field-Induced Layering of Colloidal Crystals " *Science*, vol. 272, pp. 706, 1996.

[15] S.-R. Yeh, M. Seul, and B. I. Shraiman, "Assembly of ordered colloidal aggregrates by electric-field-induced fluid flow," *Nature* vol. 386, pp. 57, 1997.

[16] F. Nadal, F. Argoul, P. Hanusse, B. Pouligny, and A. Ajdari, "Electrically induced interactions between colloidal particles in the vicinity of a conducting plane," *Phys. Rev. E*, vol. 65, pp. 061409, 2002.

[17] P. J. Sides, "Calculation of Electrohydrodynamic Flow around a Single Particle on an Electrode," *Langmuir*, vol. 19, pp. 2745, 2003.

[18] A. Hashimoto, K. Suenaga, A. Gloter, K. Urita, and S. Iijima, "Direct Evidence for Atomic Defects in Graphene Layers," *Nature*, vol. 430, pp. 870, 2004.

[19] G.-D. Lee, C. Z. Wang, E. Yoon, N.-M. Hwang, D.-Y. Kim, and K. M. Ho, "Diffusion, Coalescence, and Reconstruction of Vacancy Defects in Graphene Layers," *Phys. Rev. Lett.*, vol. 95, pp. 205501, 2005.

Chapter 8 Conclusion

8.1 Conclusions

The purpose of this thesis was to study the mechanisms underlying crystallization. Crystallization begins with nucleation and subsequently proceeds by crystal growth. In this thesis, issues including nuclei structure, nucleation route, growth kinetics, and the properties of defects were studies.

First, the structure of crystal precritical nuclei was studied. It was found that the structure of precritical nuclei is liquid-like rather than crystal-like at an earliest stage. In the following growth, nuclei undergo a transition in structure from the liquid-like to the crystal-like. In our experiments, the transition is a continuous process, that is, the component of crystal in the precritical nuclei increases gradually with the nuclei size. The analysis suggests that a continuous structure transition is favored than a sharp transition due to its lower nucleation energy barrier. Nuclei become entirely ordered

only when they exceed a critical size, namely the transition size. At high supersaturations, when the transition size becomes small enough, nuclei are formed with ordered structure from the beginning. It means that the nucleation route predicted by the classic nucleation theory tends to proceed at high supersaturations.

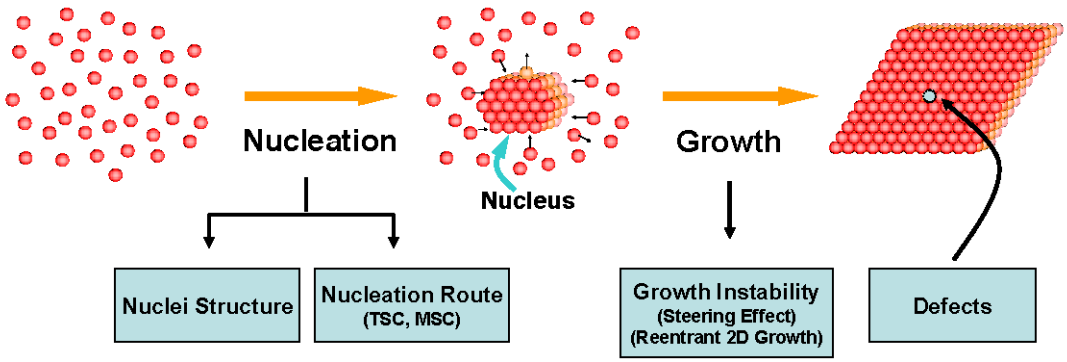

Figure 8.1 Issues studied in this thesis

Furthermore, crystallization via an amorphous precursor, the so-called multi-step crystallization (MSC), was studied quantitatively. In MSC, amorphous dense droplets are first nucleated from the mother phase. Subsequently, a few unstable sub-crystalline nuclei are created simultaneously by fluctuation from the tiny dense droplets. This picture is different from previous theoretical predictions. It is necessary for these crystalline nuclei to reach a critical size N^*_{crys} to become stable. However, in contrast to sub-crystalline nuclei, a stable mature crystalline nucleus is not created by fluctuation, but by coalescence of sub-crystalline nuclei. This is unexpected theoretically. To accommodate a mature crystalline nucleus larger than the critical size

N^*_{crys}, the dense droplets have to first acquire a critical size N^*. This implies that only a fraction of amorphous dense droplets can serve as a precursor of crystal nucleation. As an outcome, the overall nucleation rate of the crystalline phase is, to a large extent, determined by the local nucleation rate of crystals in the dense droplets. Most interestingly, the investigation revealed that MSC has advantages in producing defect free crystals.

To address the nucleation rate of MSC, a mathematical method is developed to calculate the local nucleation rate of the crystals in the amorphous precursor, which is not accessible to conventional methods. This local nucleation rate has never been dealt with experimentally due to the difficulties of *in-situ* observation. With the local crystal nucleation rates, the supersaturation for crystallization and the crystal-liquid interfacial free energy in the amorphous precursor are evaluated. The analysis suggested that the real crystal-liquid interfacial free energy should be much smaller than the estimate.

Because of the attraction between the incoming particles and the growing front, incoming monomers are collected preferentially by step protrusions, giving rise to the formation of step peaks, the so-called steering effect. However, the situation becomes complicated in the case of incoming dimers. The stronger attraction of the incoming dimers to the existing step particles induces an additional interlayer mass transport which tends to smoothen out the local step peaks. The long term effect of the interplay between the steering effect and the smoothing effect is that the local small step peaks

are smoothened out and the large global step protrusions are developed. Based on our observations, it was suggested that the smoothing effect may plays a key role in producing a smooth growth at low temperatures in epitaxial growth.

Behavior of defects has great impact on the properties of materials. In my studies, configuration and diffusion of crystal defects are studied in the two-dimensional colloidal model system. Monomer vacancies are immobile and have identical symmetry with the underlying triangular lattice. Both dimer vacancies and trimer vacancies have two different configurations, and the configurations with higher symmetry are more stable. Dimer vacancies in our experiments exhibit the highest diffusivity, whereas the global diffusion of vacancies of larger clusters, such as trimer vacancies, is inhibited. Compared with previous studies, it is found that defect dynamics is strongly dependent on the nature of the interaction potential.

These studies offer new insight into the understanding of the crystallization which proceeds in atomic systems or protein solutions. From these studies, we can see that colloidal systems can serve as a good tool in studying phase transitions and other collective behaviors of atoms or molecules.

8.2 Recommendation for Future Study

The liquid-like structure of precritial nuclei as discussed in Chapter 3 has great effect in reducing the nucleation energy barrier. However, a quantitative study of the reduction of the nucleation energy barrier is absent due to the difficulty of

quantitatively measuring the line tension, because in our system, the interaction acting between colloidal particles has so far not been completely understood. In this case, simulation may offer an alternative approach to this issue.

There is a good deal of evidence which suggests that crystallization proceeding through a metastable amorphous phase may be a widespread mechanism. However, no effort has been devoted to establish a quantitative model to describe it. CNT is still the most often adopted theory in practice. Further work is necessary to develop a theoretical model concerning MSC. However, this is a big challenge.

In practice, heterogeneous nucleation occurs more frequently than homogeneous nucleation. Therefore, it is also of great importance in future to conduct study on heterogeneous multistep crystallization. It is important to understand how impurities or substrates will affect the mechanism of MSC.